İSTANBUL UNIVERSITY CERRAHPAŞA

ORIGINAL ARTICLE
Electrica 2023; 23(3): 550-569

Hybridizing of Whale and Moth-Flame Optimization Algorithms-Based Type-2 Fuzzy Lead-Lag Unified Power Flow Controller Damping Controller Design for Improvement of Transient Stability

Sanat Kumar Barik[1,2], Sangram Keshori Mohapatra[1,2]

[1]Department of Electrical Engineering, SEC, Mayurbhanj, BPUT,Rourkela, Odisha, India
[2]Department of Electrical Engineering, GCE, Keonjhar, Odisha, India

Cite this article as: S. Kumar Barik and S. Keshori Mohapatra, "Hybridizing of whale and moth-flame optimization algorithms-based type-2 fuzzy lead-lag unified power flow controller damping controller design for improvement of transient stability," *Electrica*, 23(3), 550-569, 2023.

ABSTRACT

This article presents the design of unified power flow controller (UPFC) damping controllers based on Proportional-Derivative (PD)-type lead-lag (PD type LL) controllers for dampening low-frequency oscillations in a power system. The proposed PD type Lead Lag based UPFC uses hybridized of Whale and Moth-Flame Optimization Algorithms (WMFOA) to tune controller parameters is compared with MFO, WMFOA, and particle swarm optimization (PSO) tuned controllers for damping low frequency oscilliations. The eigenvalue analysis of time domain simulation has been demonstrated to show the effectiveness of transient stability improvement of PD type LL UPFC controller of the power system. The results analysis reveals that hybridizing of WMFOA tuned WMFOA PD type LL UPFC has excellent capability in damping power system low-frequency oscillations. The same test model type-2 fuzzy lead-lag-based UPFC damping controller transient stability improvement performance is compared to PD type LL controller of the same power system. It is demonstrated with four alternative control signal-based UPFC damping controllers are evaluated under a variety of disturbances and variation of parameters of the power system. The damping function of the UPFC with various alternative control signals is investigated using a linearized modified Phillips–Heffron model of a power system with a UPFC controller implemented.

***Index Terms*—**Hybridizing of whale and moth-flame optimization algorithm, PD type Lead Lag, type-2 fuzzy lead-lag controller, unified power flow controller.

I. INTRODUCTION

In the present day, the power system is being forced to run at or close to its stability limitations due to the fast-rising load demand. Moreover, a lack of resources prevents the development of transmission and generation. As a result, poorly linked tie lines in the interconnected power system exhibit low-frequency oscillation. If these weakly connected tie lines are not appropriately damped, the oscillation will expand and eventually separate the system, which would result in synchronism loss [1]. The unified power flow controller (UPFC) is one of the effective Flexible AC transmission system (FACTS) devices which can control the modulation of bus voltages, increase the power transfer limits during steady state, transmission line reactance, and increase the damping of power system oscillation. The main advantage of the UPFC controller is that it can control active and reactive power flow, impedance and voltages of the transmission line of the power system independently or simultaneously [2, 3]. The dynamic models of UPFC-based designs make better controllers for the power system's power flow, voltage regulation, and damping controls [2, 3]. According to studies in the literature, the UPFC is one of the FACTS devices with great flexibility and various control capacities for series compensations, voltage control and phase shifts of the trasmission line [3-5]. It has been attempted to improve the stability of the power system by using UPFC with Proportional integral Derivative (PID) and Power oscillation damping (POD) controller of the power system [6]. The transient stability improvement with UPFC control employing transient energy function and sliding mode observer has been discussed [7]. A unified power flow controller's design for the Direct current (DC)-link capacitor using dynamic control and transient performance has been investigated for stabilization of Alternating Current (AC) transmission system [8]. The power flow calculation methods for power systems with unique structures, control analysis, operation, and planning of UPFCs, as well as, a variety of systems and approaches have been discussed [9]. The UPFC has made an attempt to adhere to the practical application requirements in the transmission line of the power system [10]. A complete analysis of the power

Corresponding author:
Sangram Keshori Mohapatra

E-mail:
sangram.muna.76@gmail.com

Received: December 14, 2022

Accepted: April 17, 2023

Publication Date: July 17, 2023

DOI: 10.5152/electr.2023.22221

injection method taking into consideration four control modes to control the voltage, active, and reactive power flow in transmission lines was done using the Newton–Raphson load flow algorithm [11]. The power system has attempted a direct Lyapunov theory-based method for power oscillation damping through stable finite-time control of UPFC [12]. The adaptive input–output feedback linearization control-based damping of low-frequency oscillations in UPFC based multi-machine multi power systems has been analysed [13]. The power system stability enhancement in UPFC based multimachine power system using linear quadratic regulator techniques has been discussed [14]. The control action and parameter optimization of UPFC-based lead-lag controller has been investigated in the study to enhance dynamic stability with regard to damping of electromechanical oscillations in power systems [15]. The effeteness of dynamic stability analysis has been carried out under different disturbances like change input prime mover, wide range of loading condition, and change in line reactance of single-machine infinite bus (SMIB) power system. It has been attempted the optimal location and capacity on UPFC based chaotic krill herd blended runner root algorithm for improving dynamic stability in power system [16]. The modeling and analysis of UPFC embedded system operation rules for global and local power flow under typical operation conditions have been studied in the modern power system [17]. Wang has presented a linearized Phillips–Heffron model of a power system with UPFC based controller but its main demerit is that it lacks a systematic approach for designing damping controllers of the systems [18]. A designed controller on phase compensation is not a suitable UPFC control approach as the operating points of a power system change significantly and randomly. According to studies, several researchers have used UPFC and neural network methods [19] and robust control approaches to improve system damping performance [20]. Neural network predictive control of UPFC for improving transient stability performance of power system [21]. Researchers have proposed a fuzzy logic-based damping control technique for UPFC in multimachine power systems [22]. Enhancement of small signal stability of power system using UPFC-based damping controller with novel optimized fuzzy PID controller [23]. A fuzzy-based UPFC with hybrid energy storage has been designed with coordination control to improve the stability of the power system dynamics [24]. The transient stability is improved by the using fuzzy logic and the ANFIS approach in the UPFC of the ANFIS technique has been attempted [25, 26]. The fuzzy logic controller based enhances the performance of the PID controller and permits small adjustments to the system parameters has been discussed in the literature review [27-29]. The fuzzy logic based PID controller can effectively implement the all-nonlinear system for the formulation of problems by appropriate selection of fuzzy parameters in the system [30]. The heuristic optimization-based UPFC-based damping controller has been attempted by the researchers to enhance power system stability in various power systems by using gravitational search algorithm, particle swarm optimization, genetic optimization, chaotic optimization algorithm, etc. [31-37]. Adaptive particle swarm optimization for simultaneous design of UPFC damping controllers [38]. In this paper, the hybrid whale optimization algorithm (WOA) with Moth-Flame Optimization (MFO) algorithm (WMFOA) is employed for the optimal solution of the power system problem in UPFC-based controller in the power system [39]. The MFO is a widely used metaheuristic optimization technique with a low computational complexity [40, 41, 42]. The spiral motion of moths around light sources at night served as its model. The MFO process is a very effective global search technique for searching the search space and choosing the best outcome, but its primary disadvantage is that it suffers from inadequate exploitation and an imbalance between search strategies. The WOA is based on the social behavior of humpback whales that engage in hunting and it consists of three operators such as simulating the search for prey, encircling prey, and bubble net foraging. Although this WOA search strategy has offered enough exploitation for many optimization problems, it has been not able to meet the required demands of exploration during complex optimization problems [43, 44]. Therefore, the WOA and MFO algorithms have been hybridized for resolving the power system optimization problem. It is found that the proposed hybrid optimization technique WMFOA performed the most efficient method for solving different optimization issues of the system [39]. The hybrid of WMFOA design type-2 fuzzy lead-lag (T2FLL)-based UPFC damping controller has been attempted for transient stability improvement of the power system. The limitation of the proposed methodology is that it may not be exactly suited for all types of power system problems. Also, the design of T2FLL controller is more complex and need some extensive knowledge in the fuzzy logic system. There have been several optimization techniques proposed for various power system problems however no single optimization technique is perfectly suitable for all power system problems. The initial settings for the PSO, WOA, MFO, and WMFOA optimization algorithms are made in order to solve the optimization problem and determine the optimal tuning controller parameters in the power system. The proposed test model is demonstrated by using PSO, WOA, MFO, and WMFOA optimization techniques separately in PD-type lead-lag (PD type LL)-based UPFC damping controller of the system. It is observed that performances of transient stability improvement superior in WMFOA optimized UPFC-based PD type LL controller as compared with WOA, MFO, and PSO optimized design of the same controller and same power system. The proposed WMFOA optimized design of UPFC-based PD type LL controller transient performances are compared with the T2FLL controller of UPFC-based same power system mode under different disturbances of the system. The key investigations of the proposed work are given as follows:

1. A systematic approach for modeling a UPFC controller in a SMIB power system has been established in MATLAB/SIMULINK platform. The linearized modified Heffron–Phillips simulation model of the SMIB UPFC-based controller has been developed for the analysis of enhancing the small signal stability of the power system.
2. The performance of WMFOA-based design UPFC PD type LL controller has been evaluated to compare with WOA, MFO, and PSO optimization technique-based same controller and same power system. The optimization techniques formulated as optimization problem of ITAE objective function to find out the controller parameters separately by employing the WOA, MFO, PSO, and WMFOA techniques. It has been observed that WMFOA optimized PD type LL UPFC-based damping controller shows good performance in damping low-frequency oscillations and stabilizes the system as compared to WOA, MFO, and PSO optimized of the same controller of the power system.
3. The eigenvalue analysis of time domain simulation has been demonstrated to show the effectiveness of transient stability improvement of PD type LL UPFC controller power system. The results analysis reveals that WMFOA-tuned PD type LL UPFC has excellent capability in damping power system low-frequency oscillations and improved greatly the transient stability of the power system.

4. The second part of the analysis can be demonstrated in T2FLL-based UPFC controller under different conditions of control and disturbances to check the effectiveness and robustness of transient stability of the system. It shows that T2FLL-based UPFC controller performed superior as compared to PD type LL controller of the same power system.
5. It is also discussed that the system performance analysis under different disturbances and variation of parameters conditions shows that m_B-based UPFC controller is superior as compared to δ_B, δ_E, and m_E-based UPFC T2FLL controller of the same power system.

II. MODELING THE POWER SYSTEM WITH UPFC

Fig. 1 illustrates the SMIB with a UPFC-based damping controller to study the stability of the power system.

The proposed test model includes the excitation transformer, boosting transformer, two voltage source converters, and DC link capacitor. One of the two parallel transmission lines is connected to the UPFC controller which manages both active and reactive power. A series transformer connects one voltage source converter to the transmission line, while a shunt transformer connects a second converter parallel to the line. A DC link capacitor is used to link the series and shunt converters together. The converter's series sections inject a controllable voltage at the power frequency which regulates the magnitude and power factor angle of line currents. The actual power transmission between the converter's series and shunt components takes place through a massive DC link converter. The system considers the excitation, boosting, amplitude modulation ratio, and phase angle of the four input control signals. The implements of IEEE-STIA excitation system model is used in the proposed power system.

A. Non-Linear Equations

In order to obtained the non-linear differential equations for the UPFC-based SMIB power system by neglecting the resistances of the system's components such as the synchronous generator, transformer, transmission line, series, and shunt transformer. Here the transient is related to the UPFC transformers, transmission lines, and the stator of the synchronous generator. The system with UPFC's nonlinear dynamic model is shown below [29, 30].

$$\dot{\delta} = \omega_{\circ}\left(\omega - 1\right) \tag{1}$$

$$\omega^{"} = \frac{\left(P_m - P_e - D\Delta\omega\right)}{M} \tag{2}$$

$$E_q^{'} = \frac{1}{T_{do}^{'}}\left[-E_q + E_{fd}\right] \tag{3}$$

$$E_{fd}^{'} = \frac{K_A}{1+ST_A}\left[-V_{ref} - V_t\right] \tag{4}$$

$$V_{dc} = \frac{3m_E}{4C_{dc}}\left(I_{Ed}Sin\delta_E + I_{Eq}Cos\delta_E\right) + \frac{3m_B}{4C_{dc}}\left(I_{Bd}Sin\delta_B + I_{Bq}Cos\delta_B\right) \tag{5}$$

where

$$P_e = V_{td}I_{td} + V_{tq}I_{tq} \tag{6}$$

$$E_q = E_q^{'} + \left(X_d - X_d^{'}\right)I_{td} \tag{7}$$

$$V_t = V_{td} + jV_{tq} \tag{8}$$

$$V_t = X_q I_{tq} \tag{9}$$

$$V_{tq} = E_q^{'} - X_d^{'}I_{td} \tag{10}$$

$$I_{td} = I_{tld} + I_{Ed} + I_{Bd} \tag{11}$$

$$I_{tld} = \frac{X_E}{X_T}I_{Ed} + \frac{1}{X_T}\frac{m_E V_{dc}}{2}Cos\delta_E - \frac{1}{X_T}V_b Cos\delta \tag{12}$$

$$I_{tlq} = \frac{X_E}{X_T}I_{Eq} - \frac{1}{X_T}\frac{m_E V_{dc}}{2}Sin\delta_E + \frac{1}{X_T}V_b Sin\delta \tag{13}$$

$$I_{Ed} = \frac{\left(X_{dT} + X_{BB}X_{b3}\right)}{X_{dE}}V_b Cos\delta - \frac{\left(X_{dT} + X_{BB}X_{b2}\right)}{X_{dE}}\frac{m_E V_{dc}}{2}Cos\delta_E + \frac{X_{BB}}{X_{dE}}E_q^{'} - \frac{X_{dT}}{X_{dE}}\frac{m_B V_{dc}}{2}Cos\delta_B \tag{14}$$

$$I_{Eq} = \frac{\left(X_{qT} + X_{BB}X_{a3}\right)}{X_{qE}}V_b Sin\delta - \frac{\left(X_{qT} + X_{BB}X_{a2}\right)}{X_{qE}}\frac{m_E V_{dc}}{2}Sin\delta_E - \frac{X_{qT}}{X_{qE}}\frac{m_B V_{dc}}{2}Sin\delta_B \tag{15}$$

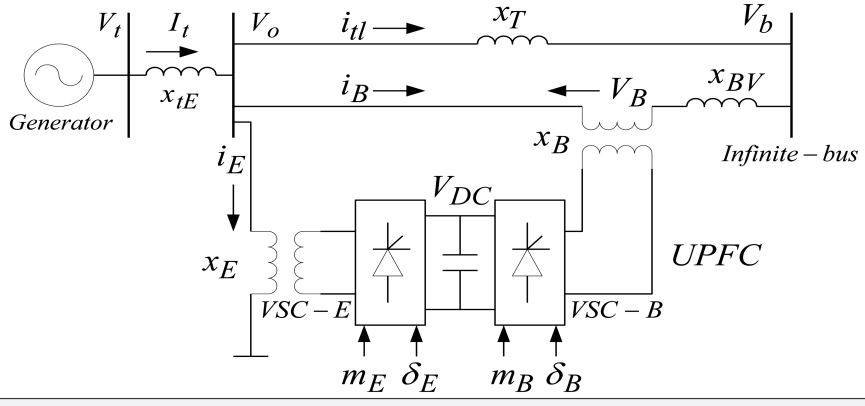

Fig. 1. SMIB with UPFC controller. SMIB, single-machine infinite bus; UPFC, unified power flow controller.

$$I_{Bd}=\frac{1}{X_{dE}}\left(X_E E_q^{'}+\left(X_{b1}-X_E X_{b2}\right)\right)\frac{m_E V_{dc}}{2}Cos\delta_E + \frac{\left(X_{b3}X_E-X_{b1}\right)}{X_{qE}}V_b Cos\delta + X_{b1}\frac{m_B V_{dc}}{2}Cos\delta_B \quad (16)$$

$$I_{Bq}=\frac{1}{X_{qE}}\left(\begin{array}{c}\left(X_{a1}-X_E X_{a2}\right)\frac{m_E V_{dc}}{2}Sin\delta_E \\ +\frac{\left(X_{a3}X_E-X_{a1}\right)}{X_{qE}}V_b Sin\delta \\ +X_{a1}\frac{m_B V_{dc}}{2}Sin\delta_B\end{array}\right) \quad (17)$$

The variables used in the earlier equations are defined as:

$$X_{qT}=X_q+X_{tE};X_{ds}=X_{tE}+X_d^{'}+X_E;$$

$$X_{qs}=X_q+X_{tE}+X_E;X_{a1}=\frac{\left(X_{qs}X_T+X_{qT}X_E\right)}{X_T};$$

$$X_{a2}=1+\frac{X_{qT}}{X_T};X_{a3}=-\frac{X_{qT}}{X_T};X_{b1}=\frac{\left(X_{ds}X_T+X_{dT}X_E\right)}{X_T};$$

$$X_{b2}=1+\frac{X_{dT}}{X_T};X_{b3}=\frac{X_{dT}}{X_T}$$

The equation for the real power balance between the series and shunt converters is as follows:

$$R_e\left(\overline{V_B}\overline{I_B}^{*}+\overline{V_E}\overline{I_E}^{*}\right)=0 \quad (18)$$

B. Linearized Equations

An electromechanical mode damping stabilizer is generally designed using a linearized incremental model with a focus on an operational point. The non-linear equations describing the operational state of the power system are linearized to produce the Phillips–Heffron model of the power system including the FACTS controller [34]. Following are the linearized expressions:

$$\Delta\ddot{\delta}=\omega_{\circ}\Delta\omega \quad (19)$$

$$\Delta\ddot{\omega}=\frac{\left(\Delta P_m-\Delta P_e-D\Delta\omega\right)}{M} \quad (20)$$

$$\Delta E'=\frac{\left(-\Delta\ddot{E}_q+\Delta E_{fd}\right)}{T_{do}^{'}} \quad (21)$$

$$\Delta\ddot{E}_{fd}=\frac{-\Delta E_{fd}+K_A\left(\Delta V_{ref}-\Delta V_t\right)}{T_A} \quad (22)$$

$$\Delta\ddot{V}_{dc}=K_7\Delta\delta+K_8\Delta E_q^{'}-K_9\Delta V_{dc}+K_{ce}\Delta m_E+K_{c\delta e}\Delta\delta_E+K_{cb}\Delta m_B+K_{c\delta b}\Delta\delta_B \quad (23)$$

where

$$\Delta P_e=K_1\Delta\delta+K_2\Delta E_q^{'}+K_{pe}\Delta m_E+K_{p\delta e}\Delta\delta_E+K_{pb}\Delta m_B+K_{p\delta b}\Delta\delta_B+K_{pd}\Delta V_{dc}$$

$$\Delta E_q=K_4\Delta\delta+K_3\Delta E_q^{'}+K_{qe}\Delta m_E+K_{q\delta e}\Delta\delta_E+K_{qb}\Delta m_B+K_{q\delta b}\Delta\delta_B+K_{qd}\Delta V_{dc}$$

$$\Delta V_t=K_5\Delta\delta+K_6\Delta E_q^{'}+K_{ve}\Delta m_E+K_{v\delta e}\Delta\delta_E+K_{vb}\Delta m_B+K_{v\delta b}\Delta\delta_B+K_{vd}\Delta V_{dc}$$

Fig. 2 shows the equivalent block diagram model. The magnitude and phase angle of the series injected voltage and shunt injected current can be changed by varying m_B, δ_B, m_E, and δ_E, respectively.

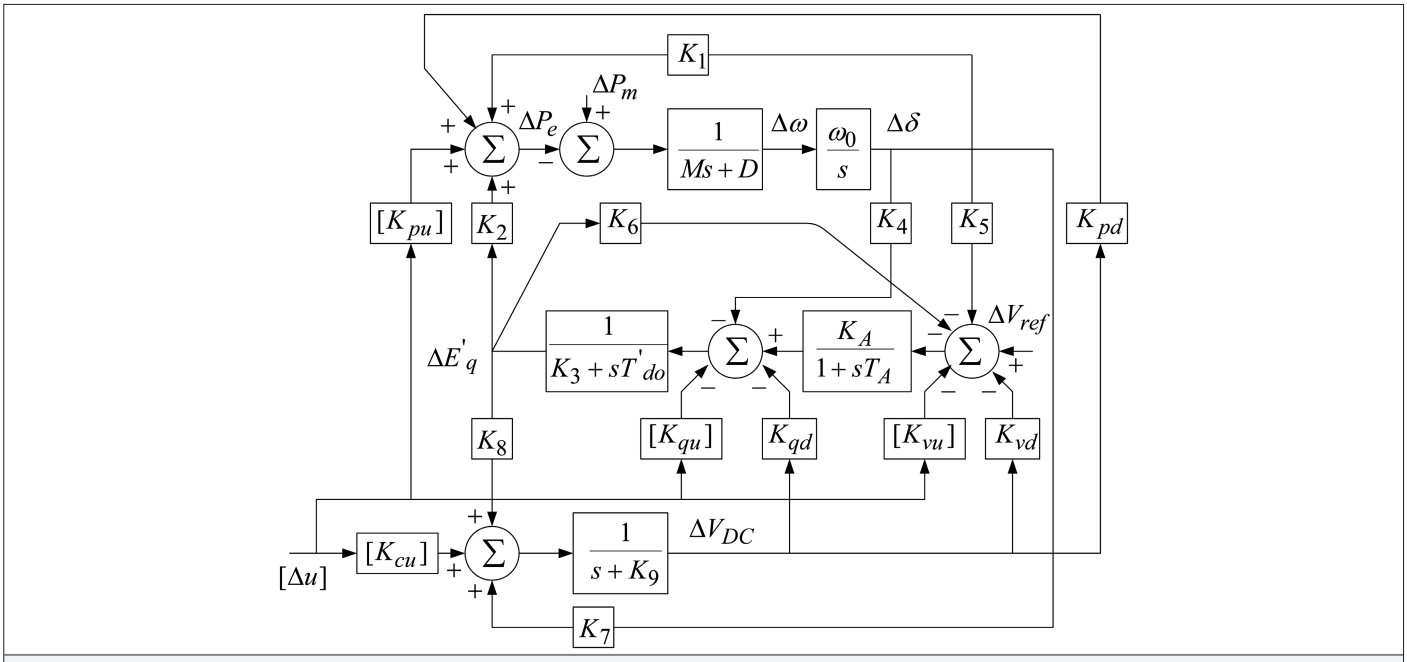

Fig. 2. Modified Heffron–Phillips model of SMIB system with UPFC controller. SMIB, single-machine infinite bus; UPFC, unified power flow controller.

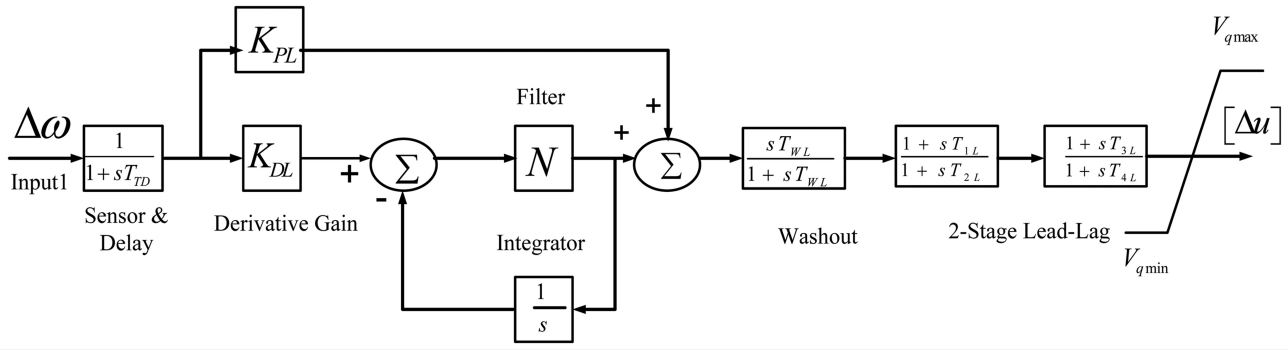

Fig. 3. PD type LL UPFC-based supplementary damping controller. PD type LL, PD-type lead-lag; UPFC, unified power flow controller

The magnitude of the series injected voltage, the phase angle of the series injected voltage, the output voltage of the shunt converter, and the phase angle of the output voltage of the shunt converter are changed by changing m_B, δ_B, m_E, and δ_E, respectively. The series and shunt converters must be regulated synrchronously to ensure that the real power output of the shunt converter equals the real power input to the series converter. This symmetry is maintained because the DC voltage remains constant. In Fig. 2, the row vectors $\left[K_{pu}\right]$, $\left[K_{qu}\right]$, $\left[K_{vu}\right]$, and $\left[K_{cu}\right]$ are defined as follows:

$$\left[K_{pu}\right]=\left[K_{pc} \quad K_{p\delta e} \quad K_{pb} \quad K_{p\delta b}\right],$$

$$\left[K_{qu}\right]=\left[K_{qe} \quad K_{q\delta e} \quad K_{qb} \quad K_{q\delta b}\right]$$

$$\left[K_{vu}\right]=\left[K_{ve} \quad K_{v\delta e} \quad K_{vb} \quad K_{v\delta b}\right],$$

$$\left[K_{cu}\right]=\left[K_{ce} \quad K_{c\delta e} \quad K_{cb} \quad K_{c\delta b}\right]$$

The control vector $\left[\Delta u\right]$ is the column vector defined as follows:

$$\left[\Delta u\right]=\left[\Delta m_E \quad \Delta\delta_E \quad \Delta m_B \quad \Delta\delta_B\right]^T \tag{24}$$

where

Δm_B = series converter of variation of modulation index m_B

$\Delta\delta_B$ = variation of phase angle of the injected voltage,

Δm_E = shunt converter of variation of modulation index m_E

$\Delta\delta_E$ = shunt converter of variation of phase angle

III. THE PROPOSED APPROACH

A. Structure of UPFC-Based Damping Controller

The two type of control structure for UPFC-based damping controller design are taken into considered in the propesd power system's for analysis of transient stability. In order to analyze the transient stability of the SMIB power system, the PD type LL based UPFC damping controller as depicted in Fig. 3 is initially taken into consideration. The second controller as shown in Fig. 4 is T2FLL-based UPFC controller structure of the SMIB power system. The detailed analysis of PD type LL and T2FLL controller-based UPFC supplementary damping controller is discussed in the section "PD type LL Controller and Type-2 Fuzzy Logic Lead-Lag Controller".

1) Type-2 Fuzzy Logic Overview: The conventional fuzzy logic control (FLC) is unable to improve the performance of the controller when a lot of variables are present. The effectiveness of the power system is improved through the double membership function (MF) based type-2 fuzzy logic controller. According to the current study, T2FLL designs are preferred to control the system frequency. The two types of MFs used by type-2 FLCs are upper MF (UMF) and lower MF (LMF). A barrier is produced by combining UMF with LMF. It is possible to establish a footprint of uncertainty (FOU) by using UMF and LMF only. Defuzzification, fuzzification, type reducer (TR), and knowledge base are the inherent properties present in the type-2 fuzzy act. The initial stage of FLC is fuzzification. The requisite structured fuzzy sets (FSs) are produced by processing inputs employing MFs. The linguistic factors utilized for MFs are zero [ZER], least negative [LN], least positive [LP], extreme positive [EXP], and extreme negative [EXN]. The following representations are possible for the type-2 FS:

$$FS=\left(\left(Var,a\right),\mu_U\left(Var,a\right)\right),\forall Var\in P,\forall a\in J_{Var}\left[0,1\right] \tag{25}$$

where $\mu_U\left(Var,a\right)$ represents the UMF, *Var* is the principal variable, and "*a*" is the additional variable of domain J_{Var}

The universe of discourse can be stated as follows:

$$FS=\int_{Var\in P}\int_{a\in J_{Var}[0,1]}\frac{\mu_E\left(Var,a\right)}{\left(Var,a\right)} \tag{26}$$

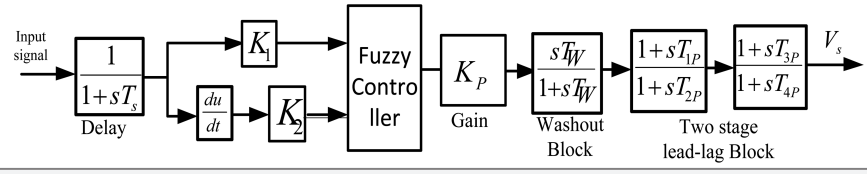

Fig. 4. Type-2 FLC LL UPFC controller. FLC, fuzzy logic control; LL, lead-lag; UPFC, unified power flow controller

where $\iint$ = Union on *ACE* and *a*

The equations now have the following forms:

$$\mu_{\bar{U}}\left(Var,a\right)=\overline{FOU\left(U\right)}\forall Var\in P,\forall a\in J_{Var}\left[0,1\right] \tag{27}$$

where J_{Var} is expressed as:

$$JVar=\left[\mu_{\bar{U}}\left(Var,a\right),\mu_{\underline{U}}\left(Var,a\right)\right]\forall Var\in P,\forall a\in J_{Var}\left[0,1\right] \tag{28}$$

The MF associated with type-I FLC promotes the formation of LMF and UMF. The interface engine and rule base are components of the knowledge base. Table I gives an example of the rule basis.

Var and *dAVar* are the individual input signals to a type-2 FLC, which produces the output y.

The characteristic of type-2 FLC is

$$LMF:forVar=\underline{LN};dVar=\underline{Z};Y=\underline{LN} \tag{29}$$

$$UMF:forVar=\overline{LN};dVar=\overline{Z};Y=\overline{LN} \tag{30}$$

The related FS firing forte is

$$\underline{f^s}=\min\left(\mu_{\overline{US}}\left(Var,a\right),\mu_{\overline{US}}\left(dVar,a\right)\right) \tag{31}$$

$$\overline{f^s}=\max\left(\mu_{\overline{US}}\left(Var,a\right),\mu_{\overline{US}}\left(dVar,a\right)\right) \tag{32}$$

$$F^s=\left[\underline{f^s},\overline{f^s}\right] \tag{33}$$

In order to defuzzify, type-2 FS is transformed to type-1 FS using TR. Defuzzification techniques include center of sums, centroid, and Center of Sets (SOC), with SOC being the most effective one.

The output equations are as follows:

$$Y_{cos}=\sum_{s=1}^{25}\frac{F^sY^s}{F^s}=\left[Y_{m1},Y_{m2}\right] \tag{34}$$

$$Y_{m1}=\frac{\sum_{s=1}^{25}\underline{f^sy^s}}{\sum_{s=1}^{25}\underline{fy}} \tag{35}$$

TABLE I. RULE BASE OF FUZZY CONTROLLER

	$\dot{e}$				
e	**EXN**	**LN**	**ZER**	**LP**	**EXP**
EXN	EXN	EXN	LN	LN	ZER
LN	EXN	LN	EXN	ZER	LP
ZER	LN	LN	ZER	LP	LP
LP	LN	ZER	LP	LP	EXP
EXP	ZER	LP	LP	EXP	EXP

LN, least negative; LP, least positive; EXN, extreme negative; EXP, extreme positive; ZER, zero.

$$Y_{m2}=\frac{\sum_{s=1}^{25}\overline{f^sy^s}}{\sum_{s=1}^{25}\overline{fs}} \tag{36}$$

Where two MF of type-1 FLC are Y_{m1} and Y_{m2}. By averaging, type-2 FLC output can be achieved. The suggested T2FLL is set up taking into account all lead-lag controller and type-2 FLC characteristics.

B. PD type LL Controller and Type-2 Fuzzy Logic Lead-Lag Controller

Fig. 3 depicted the block diagram of PD type LL controller. It is considered as a supplementary controller for UPFC-based damping controller of the power system. The PD type LL controller model comprises various blocks such as sensor and delay, proportional gain, derivative gain, filter constant($N=100$), washout block, and a two-stage lead-lag phase compensation block. The PD type LL-based UPFC controller as shown in Fig. 3 is used by the series converter to modulate voltage [Δu] in order to make up for the phase lag between the input and output signals. Fig. 4 depicts the design of the T2FLL-based UPFC damping controller in the power system. The Type-2 fuzzy logic lead-lag UPFC-based controller is employed with input scaling factors K_1 and K_2. The T2FLL UPFC controller contains a sensor block, transport delay block, scaling factor blocks for fuzzy input, gain block, washout block, and lead-lag (LL) blocks. The FLC-based LL controller can be successfully used for all nonlinear systems, but there is no specific mathematical formulation to decide the proper choice of fuzzy parameters (such as inputs, scaling factors, MFs, and rule base). Normally these parameters are selected by using certain empirical rules and therefore may not be the optimal parameters. The improper selection of the input–output scaling factor may affect the performance of FLC to a greater extent. The performance of optimal controllers depends on the appropriate selection of optimization algorithm used for tuning the parameters. In view of the above, the input and output scaling factors of T2FLL UPFC damping controller employing hybrid MFO–WOA design for tuning the controller parameters in the system. The design controller parameters for T2FLL UPFC-based controller parameters (Ks, T1p, T2p, T3p, T4p, K1, K2) are to be determined by using the WMFOA optimization algorithm. In both the case of the controller, the washout block functions act like a high pass filter and have a time constant of Tw. The Tw is chosen as 10 seconds from a range of 1 to 20 seconds [45]. The controller employs the remote speed deviation (Δω) as the input signal but for the effective design of the controller, a suitable choice of the input signal is very important for correct control action during large disturbances [46]. Without it, steady changes in input would modify the output. The speed deviation is taken in both the case of the UPFC-based controller's input signal and its output is a change in the control vector. [Δ*u*].

C. Objective Function

The power system oscillations are caused by disturbances in the system which are decreased by using PD type LL controllers and Type-2 Fuzzy logic LL-based UPFC controllers in the power system. The power system oscillations can be affecting the speed deviation of the synchronous generator in the proposed system. In order to enhance the system's performance in terms of settling time and overshoots, this study uses the integral time absolute error (ITAE) of the speed deviations as an objective function (J).

$$J = \int_0^{tim} t\,|\Delta\omega| dt \tag{37}$$

where *tim* simulation time in seconds. The optimization of tuning controllers' parameters can be obtained by employing the optimization algorithm in the proposed SMIB power system. Therefore, to bind the parameters, the objective function needs to impose certain constraints which can be expressed as in (37) in the form of an optimization problem.

Subjected to

$$K_{PL}^{\min} \le K_{PL} \le K_{PL}^{\max}, K_{DL}^{\min} \le K_{DL} \le K_{DL}^{\max},$$

$$T_{1L}^{\min} \le T_{1L} \le T_{1L}^{\max}, T_{2L}^{\min} \le T_{2L} \le T_{2L}^{\max},$$

$$T_{3L}^{\min} \le T_{3L} \le T_{3L}^{\max}, T_{4L}^{\min} \le T_{4L} \le T_{4L}^{\max},$$

for PD type LL controller

$$K_P^{\min} \le K_P \le K_P^{\max}, K_1^{\min} \le K_1 \le K_1^{\max},$$

$$K_2^{\min} \le K_2 \le K_2^{\max}, T_{1L}^{\min} \le T_{1L} \le T_{1L}^{\max},$$

$$T_{2L}^{\min} \le T_{2L} \le T_{2L}^{\max}, T_{3L}^{\min} \le T_{3L} \le T_{3L}^{\max},$$

$$T_{4L}^{\min} \le T_{4L} \le T_{4L}^{\max}$$

for T2FLL controller

Using these optimization techniques, the damping controller's parameters are found. The optimal controller parameters often fall between these regions. [1–100] for K_{PL}, K_{DL}, K_P, [0.01 2] for K_1, K_2, T_{1L}, T_{2L}, T_{3L}, T_{4L}.

IV. OVERVIEW OF MFO AND WOA ALGORITHM

A. Moth-Flame Optimization

A recently developed metaheuristic population-based algorithm is an MFO algorithm [40]. The different types of species are present in nature where moths are one of the insects alike to butterflies. During the night time, moths are navigating in the moonlight. The moths are using a mechanism for navigation called transverse orientation. One of the best and the effective mechanism-searching processes of the moth is that it can fly in a transverse orientation. It is very effective for the moth to travel a great distance in a straight line by keeping a constant angle in relation to the moon [40, 41]. It is also observed that moths can fly spirally around the light source. This behavior of the moth is demonstrated by a theoretical model as per the reference taken in [41]. It is observed that the moth flies to search its position in the spiral path around the source of light and ultimately converges toward the source of light. The MFO algorithm is formulated whose basic principle of optimization technique is based on the movement of moth insect around the light source for searching best position in space. This activity of the moth can be modeled mathematically and the corresponding algorithm is called MFO algorithm [39-41, 42, 47]. The position of each moth in space corresponds to a variable in the problem, and each moth represents a candidate solution. in the space represents a variable in the problem. Hence, moths can fly in multi-dimension (1D, 2D, 3D) in space by changing their position vectors. The *n* and *d* number of moths and variable, respectively, can be represented in ($n \times d$) dimensional matrix form called moth matrix as per in (38).

$$M = \begin{bmatrix} m_{11}, m_{1,2}, \ldots\ldots\ldots\ldots m_{1,d} \\ m_{2,1}, m_{2,2} \ldots\ldots\ldots\ldots m_{2,d} \\ m_{3,1}, m_{3,2} \ldots\ldots\ldots\ldots m_{3,d} \\ \ldots \\ \cdot \\ m_{n,1}, m_{n,2} \ldots\ldots\ldots\ldots m_{n,d} \end{bmatrix} \tag{38}$$

The fitness values of all the moths are represented as an array and are stored in a column matrix as given below

$$OM = \begin{bmatrix} OM_1 \\ OM_2 \\ OM_3 \\ \vdots \\ \vdots \\ OM_n \end{bmatrix} \tag{39}$$

The fitness value presented as an array in the above fitness function for each moth return value. For each of the moths, there is a position vector which is entered into the fitness function. The fitness function can be evaluated as per the allotted fitness value of each moth. The flames are one of the important elements in the anticipated algorithm. The flame matrix is considered similar to an *n* number of moth matrix as given:

$$F = \begin{bmatrix} F_{1,1}, F_{1,2}, \ldots\ldots\ldots\ldots F_{1,d} \\ F_{2,1}, F_{2,2} \ldots\ldots\ldots\ldots F_{2,d} \\ F_{3,1}, F_{3,2} \ldots\ldots\ldots\ldots F_{3,d} \\ \ldots\ldots, \ldots\ldots, \\ \cdot \\ F_{n,1}, F_{n,2} \ldots\ldots\ldots\ldots F_{n,d} \end{bmatrix}, \tag{40}$$

The array matrix in (38) and (40) is taken as the same dimension.

$$OF = \begin{bmatrix} OF_1 \\ OF_2 \\ OF_3 \\ \vdots \\ \vdots \\ OF_n \end{bmatrix} \tag{41}$$

Equation (41) represents the fitness value of flames and is an array flame matrix as taken in (40). It should be observed that the difference between the moth and flame solutions is upgrading with each iteration. The search agent (moths) moves around in the search region to determine the best location for moths in the flames. When moths are flying in the search space then it may drop these flames which might be thought of as flags. The moths are search and update a flag in the search space to determine the best solution. The MFO obtains optimum value with rapid and smooth convergence. The global optimization problem of this algorithm is defined as follows:

$$MFO = (I, P, T) \tag{42}$$

There are three tuples of this algorithm used as "I" represents a function which can generate a random population. The space "P" is a

function that represents search space for moths and "T" is a function that returns a value which depends upon the termination criteria.

The systematic model of *I* with its corresponding value is given as.

$$I:\varphi \to \{M,OM\} \tag{43}$$

The main function P received the moth matrix and updated the matrix's returns to one in the final step,

$$P:M \to P \tag{44}$$

if the T function's return termination condition has been satisfied, it returns true; otherwise, it returns false, which represents as:

$$T:M \to \{true,false\} \tag{45}$$

The purpose algorithm of the earlier function can be represented as given:

M = I();

while *T(M) = false*

than M = P(M);

end

The function I used to generate initial solutions and calculate the objective function values is then the utilized with a random distribution.

The method is used for fitness value as follows:

for *i = 1: n*

for *j = 1: d*

*the fitness function M(i, j) = (ub(i) — lb(i)) * rand() + lb(i);*

end

end

OM = Fitness Function(M);

The upper bound of array *ub* and lower bound of array *lb* variables are represented in (46) and (47) which are as follows:

$$ub = \left[ub_1, ub_2, ub_2, \ldots\ldots\ldots ub_{n-1}, ub_n\right] \tag{46}$$

$$lb = \left[lb_1, lb_2, lb_2, \ldots\ldots\ldots lb_{n-1}, lb_n\right] \tag{47}$$

where *ubi and lbi* indicate the upper and the lower bound of the *i*th variable respectively.

The *P* function will be running iteratively till *T* function returns true after the initialization of the variable. It is the main function that helps to carry and move the moths around the search space. Due to the above hold-up, the algorithm has a nature of transverse orientation.

This behavior can be subjected to the position of each moth that is updated with respect to flame as per the equation

$$M_i = S\left(M_i, F_j\right) \tag{48}$$

where *S* is spiral function, M_i refers to *i*th moth, and F_j refers to *j*th flame.

The update mechanism of moths is used in a logarithmic spiral in the proposed algorithm. The main approach used by moths to update their position in this article is a logarithmic spiral path, and the selection of spiral path is dependent upon the conditions as provided below which represented by

- The moth itself should represent the starting point for its spiral's initial point.
- The position of the flame should be the ending point of its spiral.
- The search space can be taken within the limit range of spiral.

In the case of a logarithmic spiral for the proposed technique having *i*th moth and *j*th flame is defined as follows:

$$S\left(M_i, F_j\right) = D_i.e^{bt}.\cos(2\pi t) + F_j \tag{49}$$

where b is the constant that determines the shape of the logarithmic spiral path, D_i represents the distance between the *i*th moth and *j*th flame, *t* represents a random number whose value is taken in the range [−1,1]. In (49), *D* can be calculated for *i*th moth and *j*th flame by using (50) as follows:

$$\left|D_i = F_j - M_i\right| \tag{50}$$

where *Fj* = *j*th flame and *Mi* = the *i*th moth,

In (49), t is the parameter that represents the closeness next position of the moth with respect to the flame (t-1), while t (1) shows the farthest. The aforementioned proposed approach determines how the moths update their positions around flames because it is a spiral movement. A moth is not allowed to fly in the space between two flames but the spiral equation (49) allows it to fly "around" a flame. Thus, it is possible to ensure the exploration and exploitation around the search space's flames by updating the target position in relation to this matrix, which is taken into consideration in (50) [30]. As in the earlier discussion, updating the position of moths with respect to different positions in the search space may decrease to the best solution. Now to solve this problem, the following formula is used:

$$Flameno = round\left(N - 1 * \frac{N-1}{T}\right) \tag{51}$$

where in the steps of iteration, *N* is the maximum number of flames, *T* refers to the maximum number of iterations, and the number of current iterations taken in this case is 1. The formula as mentioned previously which helps in finding a balance between exploitation of the search space and exploration of the gradually decreasing number of flames.

B. Whale Optimization Algorithm

The humpback whales hunting behavior in nature is mathematically modeled in the WOA [48]. As humpback whales explore for food or prey, a whale optimization process has been established [43, 44, 49]. Whales enjoy hunting prey close to the water's surface. The production of bubbles in a circular motion controls this striking activity. Whales employ the technique of swimming around their prey in a smaller loop in order to destroy it. The position of the best pattern is initially unknown; therefore, the whales assume that the best option at present is close to the best. Following the whales in the

best places and the remaining whales make modifications to their position. When using the bubble-net attacking tactic during the exploitation phase of WOA, the two methods utilized for this are the spiral updating position and the shrinking encircling method. These approaches are given in (52) and (53).

$$\vec{F} = \left|\vec{E}.\vec{Z}^{*}(t) - \vec{Z}(t)\right| \tag{52}$$

$$\vec{Z}(t+1) = \vec{Z}^{*}(t) - \vec{C}.\vec{F} \tag{53}$$

$$\vec{Z}(t+1) = \vec{F}'.e^{kl}.\cos(2\pi l) + \vec{Z}^{*}(t) \tag{54}$$

Here, t stands for the current iteration, $\vec{Z}(t)$ for the position vector, and $\vec{Z}^{*}(t)$ for the current best solution. Equation (54) guarantees that any whale will revise its location in the proximate of the current best whale. The agent's position is updated in accordance with (54) to arrive at the best outcome. In (52), $\vec{E}$ stands for the distance between the i^{th} and the best whale that has been found so far. In (54), $\vec{F}' = \left|\overrightarrow{Z^{*}}(t) - \vec{Z}(t)\right|$ is used to calculate the distance between the i^{th} whale and the best prey up to this point, with "k" designating the contour of the logarithmic spiral and "l" being a random integer between [−1,1]. The vectors $\vec{C}$ and $\vec{E}$ operate as adjustment vectors that control where the whale will be discovered in close proximity to its prey, which are mentioned in (55) and (56) as:

$$\vec{C} = 2\vec{cr} - \vec{c} \tag{55}$$

$$\vec{E} = 2\vec{r} \tag{56}$$

where $\vec{r}$ is an arbitrary quantity nominated between 1 and 0. The optimization method results in a linear drop in the parameter $\vec{c}$ from 2 to 0. The shrinking characteristics are guaranteed as $\vec{c}$ reduces. Altercation among exploitation and exploration stage follows with linearly sinking '$\vec{c}$' as in (57).

$$\vec{c} = 2 - t\frac{2}{ITER_{MAX}} \tag{57}$$

whereas '$\vec{c}$', t, and $ITER_{MAX}$ are the distance control parameter, the current iteration, and the maximum iteration. In the WOA, the best whales are the target and the other whale have the goal of updating their positions close to the best whale. In the early stages, the finest likely search agent is unknown. Therefore, using big initial steps in modification may cause whales to be moved far from their preferred location.

V. SIMULATION RESULTS

A. Application of WMFO, MFO, WOA, and PSO Optimization Algorithm

In order to demonstrate the UPFC-based damping controller for transient stability analysis, the controller parameters for the proposed power system can be determined by using optimization techniques. The SIMULINK platform can be used to develop a simulation model of the SMIB UPFC controller in the power system. The code of the hybrid optimization techniques MFO and WOA (WMFOA) can be written the MATLAB (in .m file). The optimization process was repeated 20 times for PSO, WOA, MFO, and WMFOA algorithms. The maximum number of iterations is set to 100 and number of populations is 40 taken for individual PSO, WOA, and MFO optimization algorithms. In the hybrid MFO and WOA approach, MFO techniques are applied for 50 iterations and WOA is then employed for 50 iterations to fine-tune the best solution provided by MFO. For the excruciation of the MFO technique, a series of runs were performed to choose the algorithm parameters. The following initial parameters are used in the MFO algorithm: MFO is executed with a decrease linearly from −1 to −2, b = 1 throughout the iteration and number of populations = 40. The power system simulation model is carried out at least 20 times and the best global values for controller parameters are obtained after 20 runs of the proposed system. In the next step, WOA is applied to fine-tune controller parameters. The final controller parameters found by the MFO algorithm are used in the WOA algorithm as starting points. The WOA algorithm is implemented with the parameters presented here with maximum number of populations = 40, k = 1 and the parameter $\vec{c}$ linearly decreases from 2 to 0. The best solution corresponding to the minimum fitness values obtained among the 20 runs is chosen as controller parameters by a hybrid of MFO and WOA algorism. In the PSO algorithm, fitness values are obtained by setting the initial value of parameters such as stochastic acceleration constants (c1 = 2, c2 = 2) and inertia weight w which decreases linearly from about 0.9 to 0.4. Similarly, in the case of the MFO algorithm, initial value parameters are internal random numbers in [−1,1], constant b = 1and the variable decreases linearly from −1 to −2 in the optimization iteration process. The detailed initial parameters of PSO, WOA, MFO, and WMFOA algorithms are considered in the proposed studies. The developed simulation model of PD type LL UPFC-based UPFC controller has taken 10% increase in mechanical power input disturbance of SMIB power system. The objective function is calculated in the .m file and used in the optimization algorithm. The performance of the proposed WMFOA optimized PD type LL UPFC-based controller is compared with individual PSO, WOA, and MFO optimized PD type LL controllers of the same power system. It is clear from the Table III that m_B-based UPFC PD type LL controller the least minimum ITAE value (2.9643 × 10−4) is obtained in WMFOA optimized of controller as compared to MFO optimized PD type LL controller (4.3774×10^{-4}), WOA optimized PD type LL controller (5.1476×10^{-4}), and PSO optimized same PD type LL controller (5.7811×10^{-4}) of the same power system. It is observed that WMFOA optimized in PD type LL m_B-based UPFC damping controller the percentage reduction of ITAE value as compared to WOA, MFO and PSO optimized same controller of the same power system. The percentage reduction of ITAE value in WMFOA as compared to MFO, WOA, and PSO optimized of the same controller

TABLE II. INITIAL PARAMETERS OF OPTIMIZATION ALGORITHM

Algorithm	Parameters
PSO	$c1 = c2 = 2$
WOA	$\vec{c}$ parameters is linearly decreases from 2 to 0, $k = 1$
MFO	a decrease linearly from −1 to −2, b = 1
WMFOA	$\vec{c}$ parameters is linearly decreases from 2 to 0, $k = 1$

WOA, whale optimization algorithm; PSO, Particle swarm optimization; MFO, Moth-Flame Optimization Algorithm; WMFOA, hybridizing of Whale and Moth-Flame Optimization Algorithm.

TABLE III. PSO, MFO, WOA, AND WMFOA OPTIMIZED UPFC DAMPING PD TYPE LL CONTROLLER PARAMETERS

								ITAE $\times 10^{-4}$		
	Algorithm	K_P	K_D	***T*1s**	***T*2s**	***T*3s**	***T*4s**	**Minimum**	**Average**	**Maximum**
m_B-based	PSO	88.0212	6.5733	0.3164	0.3427	0.2247	0.2611	5.7811	6.1021	6.4406
	WOA	117.6454	10.5820	1.2411	0.9940	0.8952	0.9000	5.1476	5.8115	6.8363
	MFO	135.3507	8.4347	1.1614	0.9232	0.8842	1.4818	4.3774	5.3106	5.4021
	WMFOA	120.4771	9.5547	1.0487	0.9264	1.2421	1.3836	2.9643	3.6224	4.1302
δ_B-based	PSO	38.7489	18.3900	0.3424	0.3961	0.2397	0.4148	6.3410	6.5331	7.3051
	WOA	19.5463	14.6730	0.1053	0.2747	0.2694	0.1825	5.3300	6.8066	7.5329
	MFO	22.1150	8.8051	0.2331	0.2827	0.2107	0.2673	4.6037	5.3251	5.7742
	WMFOA	79.5428	10.5217	0.9217	1.0949	0.9280	0.9248	3.6523	4.7706	5.9043
m_E-based	PSO	7.8994	8.7759	0.3949	0.1496	0.3935	0.2888	5.9937	6.5311	7.4108
	WOA	8.3123	7.7941	0.3401	0.3360	0.6866	0.2982	5.4605	6.2358	6.9900
	MFO	14.3083	6.0927	0.2878	0.1696	0.3128	0.2669	4.9311	5.5380	6.5007
	WMFOA	123.0029	9.1762	1.1665	0.8712	0.7646	1.2128	3.1405	3.8531	4.6711
δ_E-based	PSO	22.1150	16.7511	0.2331	0.2827	0.2107	0.2673	6.5844	7.3394	7.7720
	WOA	19.5463	8.6732	0.1053	0.2747	0.2694	0.1825	5.3920	6.0145	7.0438
	MFO	23.7760	26.5511	0.1439	0.2636	0.3946	0.3886	4.7604	5.4613	5.7641
	WMFOA	24.5272	14.8034	0.3665	0.2942	0.1162	0.2951	3.8802	4.2200	4.5906

UPFC, unified power flow controller; WOA, whale optimization algorithm.

is 32.28%, 42.41%, and 48.72%, respectively. It is also observed from the Table III that WMFOA optimized in each of δ_B, m_E and δ_E control signal with PD type LL based UPFC controller has least minimum ITAE value are obtained as compared to MFO, WOA, and PSO optimized same control signal with PD Type LL controller in same power system. The percentage of reduction of ITAE value in WMFOA optimized δ_B-based UPFC PD type LL as compared to MFO, WOA, and PSO optimized of the same controller are 20.66%, 31.47%, and 42.40%, respectively. The percentage of reduction of ITAE value in WMFOA optimized m_E-based UPFC PD type LL as compared to MFO, WOA, and PSO optimized of the same controller are 36.31%, 42.45%, and 47.60%, respectively. The percentage of reduction of ITAE value in WMFOA optimized δ_E-based UPFC PD type LL as compared to MFO, WOA, and PSO optimized of the same controller are 18.49%, 28.03%, and 41.06%, respectively. It is concluded that MFOA optimized PD type LL UPFC-based controller outperforms as compared to MFO, WOA, and PSO optimized with the same controller of the power system. It is also clear from the analysis that m_B-based UPFC damping controller is superior as compared to δ_B, m_E, and δ_E-based UPFC controller of the same power system. To demonstrate the dynamic performance of m_E, δ_B, m_E, and δ_E-based UPFC PD type LL controller under 10% step mechanical power input increases the proposed power system to check the effectiveness and robustness of the system. The system dynamic responses of WMFOA optimized PD type LL-based UPFC damping controller are shown as a solid line with legend WMFOA-PD type LL. The system responses of MFO optimized PD type LL-based UPFC damping controller are shown as dash line with legend MFO-PD type LL. The system responses of WOA optimized PD type LL-based UPFC damping controller are shown as dashed-dotted lines with legend WOA-PD type LL. The system responses of PSO optimized PD type LL-based UPFC damping controller are shown as dotted lines with legend PSO-PD type LL.

1) Case I:* m_B*-Based PD type LL With UPFC Controller: In Case I, the mechanical power input 10% step increases at time t = 1sec is considered in the proposed power system. It is demonstrated under this condition of the system. The system responses of speed deviation and electrical power deviation under Case I of m_B-based PD type LL with UPFC controller of SMIB power system is shown in Fig. 5a and b. It is clear from the figures that MFO, WOA, and PSO optimization maintain the system's stability and effectively decrease power system oscillations using a PD type LL controller. However, it is evident from the figures that the system's performance under the WMFOA optimized based PD type LL controller exhibits improved damping performances as compared to MFO, WOA, and PSO optimized of the same PD type LL of the same power system.

2) Case II:* δ_B*-Based PD type LL With UPFC Controller: In Case II, the suggested power system with a 10% boost in mechanical input power in step is presented at time $t = 1$ s of the system under δ_B-based UPFC damping controller. Fig. 6a and b illustrates the system's responses to this scenario as the speed deviation and active power deviation, respectively. It is clear from the figures that transient stability improvement in WMFO optimized in PD type LL-based UPFC damping controller is superior performances as compared with WOA, MFO, and PSO optimized in the same controller and same power system.

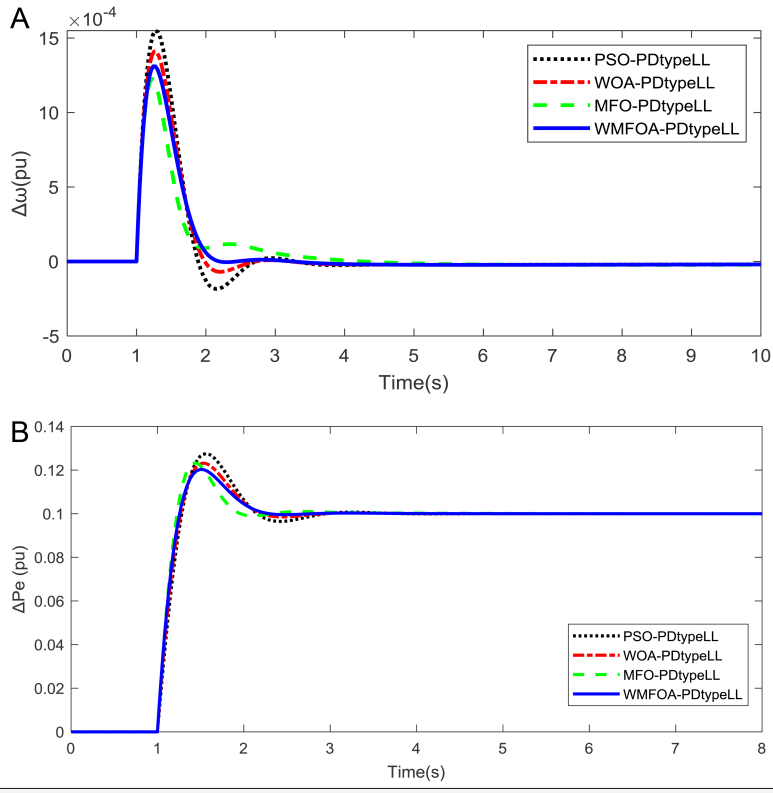

Fig. 5. (a) and (b) Speed deviation and electrical power deviation response for Case I.

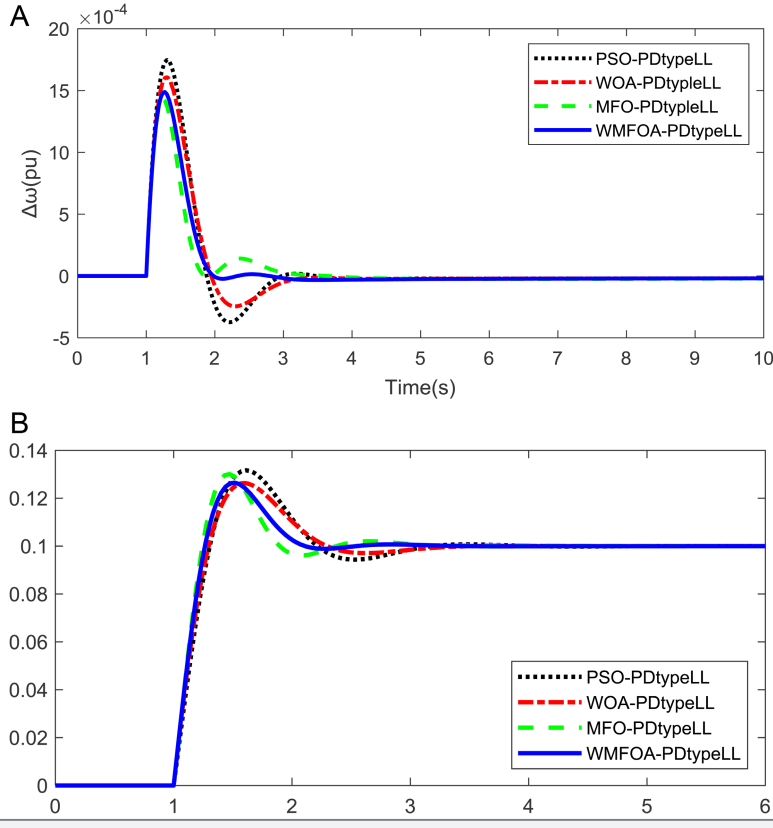

Fig. 6. (a) and (b) Speed and power deviation response for Case II.

3) Case III: ***m_E-Based PD type LL With UPFC Controller:*** Case III of the proposed system illustrated under the same contingency with a 10% increase in the mechanical input power of the generator at $t=1$ s of the system. It is demonstrated under this condition and it observed the system responses of speed deviation and active power as shown in Fig. 7a and b, respectively. It is clear from the figures that system responses under this condition of WMFOA-optimized tuning controller parameters give superior damping performances as compared to MFO, WOA, and PSO-optimized tuning controller parameters of the same system.

4) Case IV: ***δ_E-Based PD type LL With UPFC Controller:*** In Case IV, under the same contingency 10% increases the step input mechanical power to the generator with δ_E-based UPFC damping controller of the power system. The dynamic of the system response of speed deviation and power is shown in Fig. 8a and b, respectively. It is noticed that WMFOA-based optimal tuning PD type LL controller parameters performed superior transient performances as compared to MFO, WOA, and PSO-based tuning controller parameters of the system.

To check the effeteness and robustness analysis of transient stability of the proposed power system the eigenvalues are obtained during the process of optimization in the system. It is desired to shift the real part of the eigenvalue corresponding to the oscillation mode to LHS in the complex s-plane to increase the damping of system responses. This can be performed by placing the eigenvalue for the oscillation's mode on the left side of the complex plane. It is demonstrated under δ_E, m_E, δ_B, m_B-based UPFC PD type LL controller with 10% increase in mechanical input power disturbances in the proposed system. It is observed that the system eigenvalues of PSO, WOA, MFO, and WMFOA-based PD type LL UPFC controller which is shown in Table IV. It is clear from Table IV that the stability of the system is maintained as eigenvalues shift to the left-hand side of the complex s-plane. All the eigenvalues ($s=-3.31$, -4.586, -4.135, and -4.972) under m_B, δ_E, δ_B, m_E-based UPFC PD type LL controller WMFOA employed in the proposed test model. These eigenvalues are obtained in WMFOA compared with MFO, WOA, PSO-based PD type LL controller of all the eigenvalues obtained as in Table IV. It is observed from Table IV that eigenvalues are obtained under PD type LL controller used WMFOA shifted more left half of s-plane as compared to MFO, WOA, and PSO-based same controller of the power system. Therfeore, it is clear from the analysis that enhance the stability of the power system and improve the damping characteristics of electromechanical mode in WMFOA based PD type LL based controller as compared to MFO, WOA and PSO based same control structure and same power system model.

B. Analysis of Power System Stability in T2FLL Controller Under δ_E, m_E, δ_B, and m_B Based With UPFC Damping Controller

As per the prior analysis of this article, it is observed that transient stability improvement in WMFOA optimized PD type LL based UPFC damping controller superior as compared to MFO, WOA, and PSO optimized same PD type LL of the power system. The analysis of power system stability of the system T2FLL-based UPFC damping

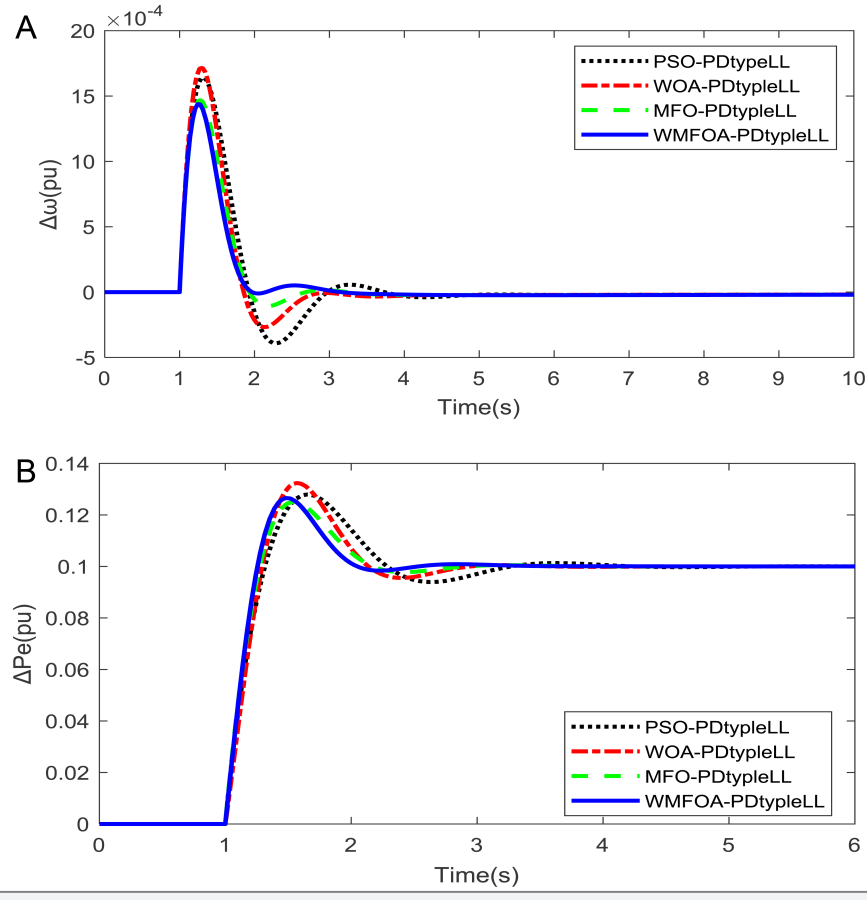

Fig. 7. (a) and (b) Speed and power deviation responses for Case III.

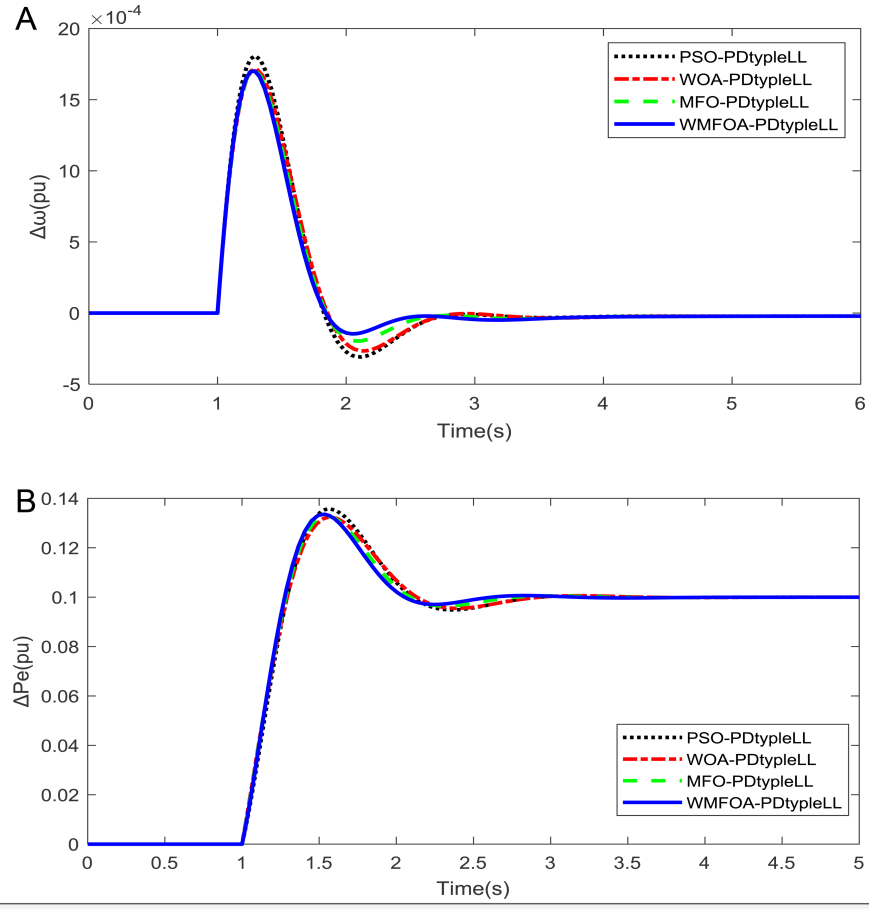

Fig. 8. (a) and (b) Speed and power deviation response for Case IV.

TABLE IV. SYSTEM EIGENVALUES UNDER 10% INCREASES IN MECHANICAL POWER INPUT USING PSO, WOA, MFO, AND WMFOA

Controller	Case I m_B	Case II δ_B	Case III m_E	Case IV δ_E
PSO-based PD type LL	−1.749 + 1.438i	−1.883 ± i2.075	−2.004 ± i1.847	−1.792 ± i1.315
WOA-based PD type LL	−2.432 ± i0.571	−3.207 ± i1.541	−3.113 ± i1.431	−3.894 ± i.816
MFO-based PD type LL	−2.773 ± i0.351	−3.914 ± i0.473	−3.782 ± i1.103	−4.256 ± i.434
WMFOA-based PD type LL	−3.31 ± i0.214	−4.586 ± i0.383	−4.135 ± i0.988	−4.972 ± i0.251

PD type LL, PD-type lead-lag; WOA, whale optimization algorithm.

TABLE V. OPTIMIZED T2FLL-BASED UPFC DAMPING CONTROLLER PARAMETERS

Damping Controller	K_1	K_2	Kp	T1s	T2s	T3s	T4s	ITAE × 10^{-4}
m_B-based	0.2721	0.6638	90.2782	0.2799	0.2705	0.2296	0.3272	1.8771
m_E-based	0.6638	0.2641	14.3083	0.2878	0.1696	0.3128	0.2669	3.0371
δ_B-based	0.3700	0.8533	45.3409	0.3478	0.3064	0.1155	0.4385	3.4153
δ_E-based	0.3531	0.7455	29.8276	0.1090	0.2463	0.2416	0.2367	3.5720

ITAE, integral time absolute error; UPFC, unified power flow controller.

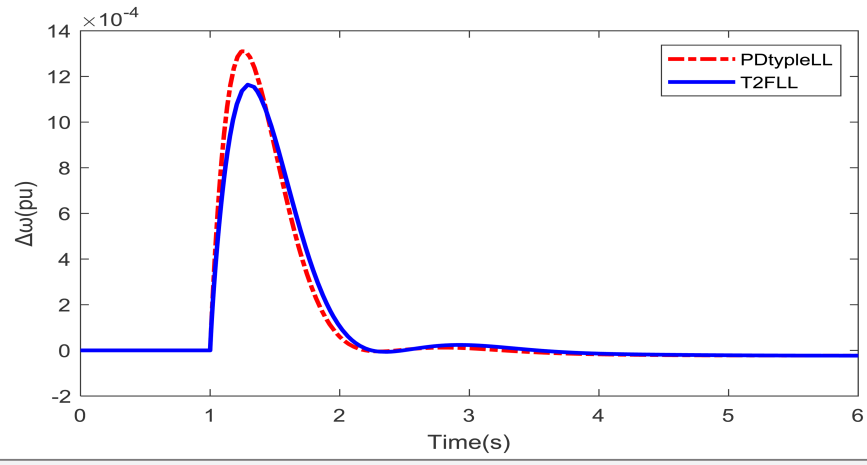

Fig. 9. Speed deviation response for Case I.

controller employed WMFOA optimization algorithm of the proposed power system. It demonstrated the power system stability analysis under m_B, δ_B, δ_E, m_E-based T2FLL UPFC damping controller in the proposed power system. In the same procedure as in the previous analysis, WMFOA optimized T2FLL UPFC-based damping controller parameters and ITAE value obtained by taking a minimum of 20 runs of the optimization process of the system. The optimization controller parameters and ITAE value are obtained under δ_E, m_E, δ_B, m_B-based T2FLL UPFC damping controller of the system as shown in Table V. It is observed from Table V that m_B, m_E, δ_B, and δ_E-based T2FLL UPFC damping controller ITAE values are 1.8771×10^{-4}, 3.0371×10^{-4}, 3.4153×10^{-4}, and 3.5720×10^{-4}, respectively. It is clear that the least value of ITAE value is obtained in m_B based T2FLL UPFC controller as compared to m_E, δ_B, δ_E-based T2FLL UPFC-based controller of the same power system. It is observed from Table V that MFOA optimized m_B- signal T2FLL based UPFC damping controller the percentage of reduction of ITAE value 38.19%, 45.03%, and 47.44%, respectively as compared to *mE*, *δB*, *δE signal* based T2FLL based UPFC controller of same power system. It is clear that m_B-based T2FLL UPFC damping controller employed MFOA optimized outperforms as compared to m_E, δ_B, and δ_E-based T2FLL UPFC damping controller of the same power system.

It can be demonstrated the power system stability analysis under different input signal of m_B, δ_E, δ_B, m_E in T2FLL based UPFC controller is applied 10% step mechanical input power increases to the generator of the power system. The dynamic system response of T2FLL UPFC-based controller performances is compared to the PD type LL UPFC-based damping controller of the same power system. Fig. 9 shows the speed deviation of system responses of m_B-based T2FLL UPFC controller compared to the PD type LL controller of the system power system. It is clear from Fig. 5 that m_B-based T2FLL UPFC controller gives better transient performances compared to m_B-based PD type LL UPFC controller of the same power system. It is demonstrated that of δ_B-based T2FLL, m_E-based T2FLL, and δ_E-based T2FLL UPFC damping controller under same disturbances taken as Case II, Case III, and Case IV of the same power system. It is observed from the demonstration that the system response of speed deviation for the cases of δ_B-based T2FLL, m_E-based T2FLL, and δ_E-based T2FLL UPFC controller are compared to same input signal *δB, mE, δE* of PD type LL based UPFC damping controller same power system. It is clear from Fig. 11 and Fig. 12 that the system responses of speed deviation in T2FLL controller performed better in terms of settling time and overshoot of the system.

1) Case V: Bulk Load Changes: In Case V, the 25% increases in step input mechanical load are applied to the generator of the power system. The system is demonstrated under this condition. The system responses of this disturbance of speed deviation m_B-based control

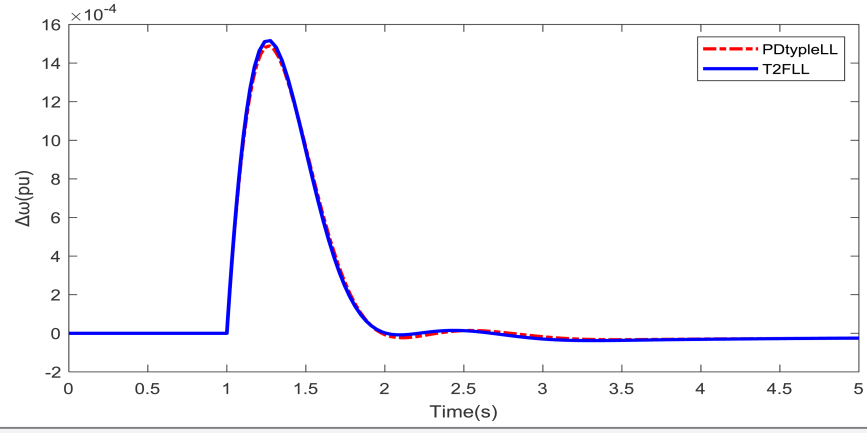

Fig. 10. Speed deviation response for Case II.

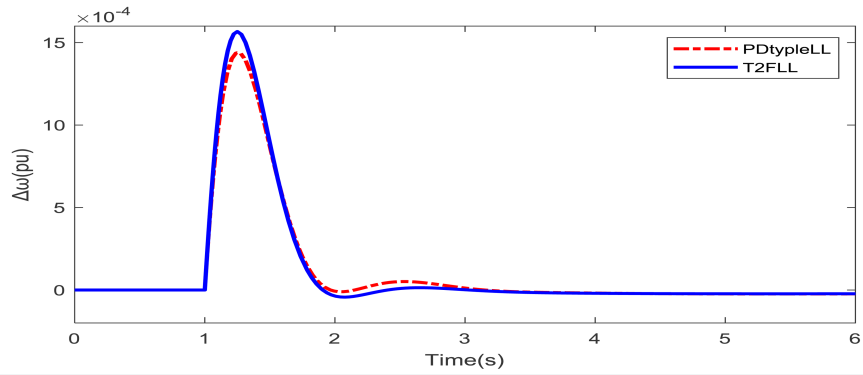

Fig. 11. Speed deviation response for Case III.

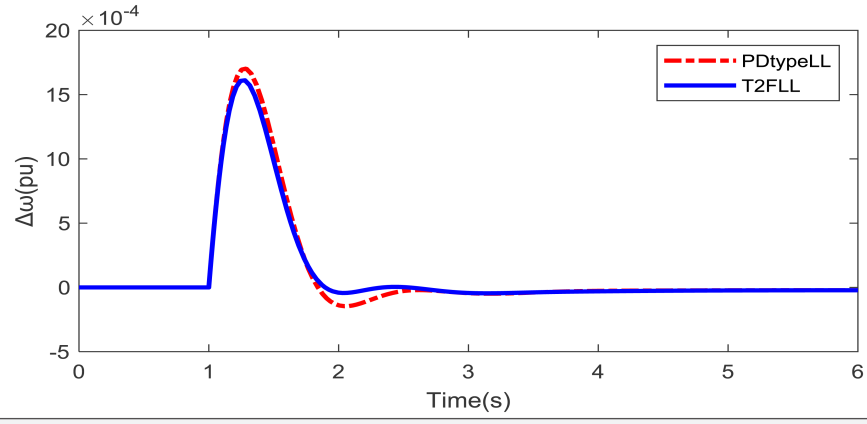

Fig. 12. Speed deviation response for Case IV.

actions using WMFOA design of PD type LL and T2FLL controller are shown in Fig. 13. It can be seen that the proposed m_B-based control T2FLL UPFC damping controller has good performance in damping low-frequency oscillations and stabilizes the system as compared to PD type LL of the same power system.

2) Case VI: Change in Mechanical Step Input Load and Reference Voltage Simultaneously: In Case VI can be demonstrated under simultaneously increasers in step load 20% and 10% decreases the Vref step load in the system. The demonstration of m_B-based control of T2FLL and PD type LL controller under this condition of the proposed system is considered. The system responses as in Fig. 14 show the speed deviation of the T2FLL and PD type LL controller of the power system. It is clear from Fig. 14 that m_B-based T2FLL UPFC damping controller gives superior transient performances as compared to PD type LL controller of the same power system.

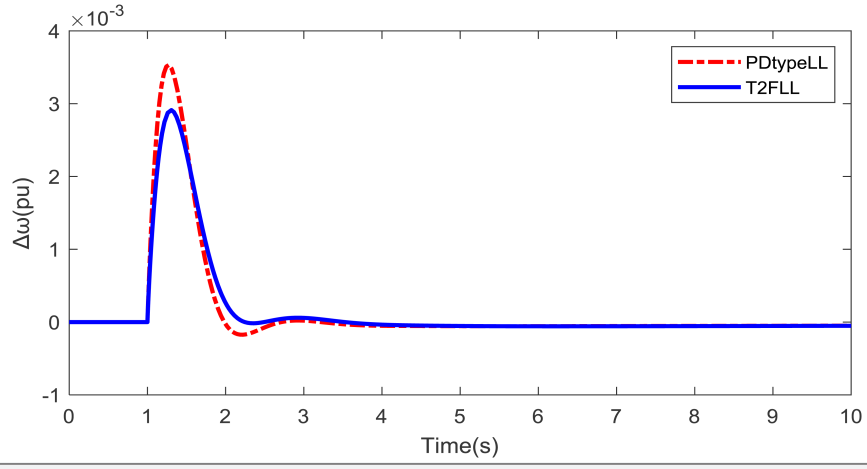

Fig. 13. Speed deviation response for Case V.

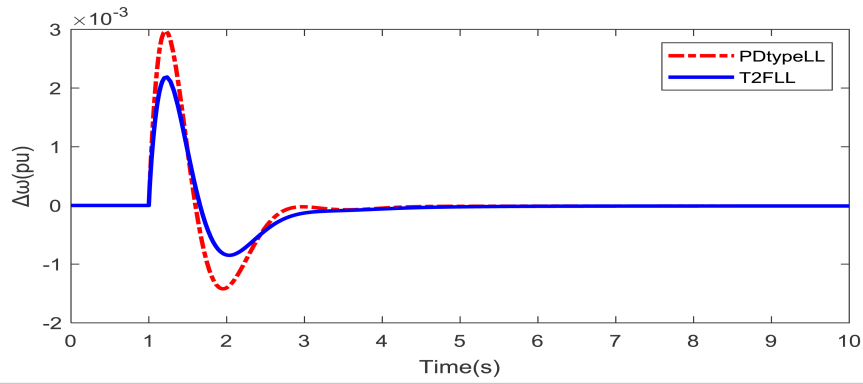

Fig. 14. Speed deviation response for Case VI.

3) Case VII: Assessment of Four Alternatives in T2FLL-Based UPFC Controller: In Case VII, it is demonstrated under two condition 10% increase in step load and 5% decreases in step load respectively in T2FLL built UPFC damping controller of the proposed power system. Fig. 15a and 13b illustrates the system's responses of speed deviation under two conditions of disturbances of the system. It is observed from the Fig. 15a and b that all four choices maintain the damping of stability performances. However, the m_B-based T2FLL UPFC damping controller is the best choice among the four alternatives.

4) Case VIII: Assessment of Four Alternatives in T2FLL-Based UPFC Controllers' Variation of Reference Voltage: To check the robustness of transient stability in T2FLL-based UPFC damping controller of the power system can be demonstrated under the disturbances of references voltage is rises to 5% at time $t=1$ sec. The system responses of speed deviation with all the four alternatives of the proposed controller are shown in Fig. 16. It is clear from the Figure-16 that m_B input signal T2FLL based UPFC damping controller exhibits better transient responses as compared to input control signals (mE. δB, δE) of T2FLL controller of same power syste.

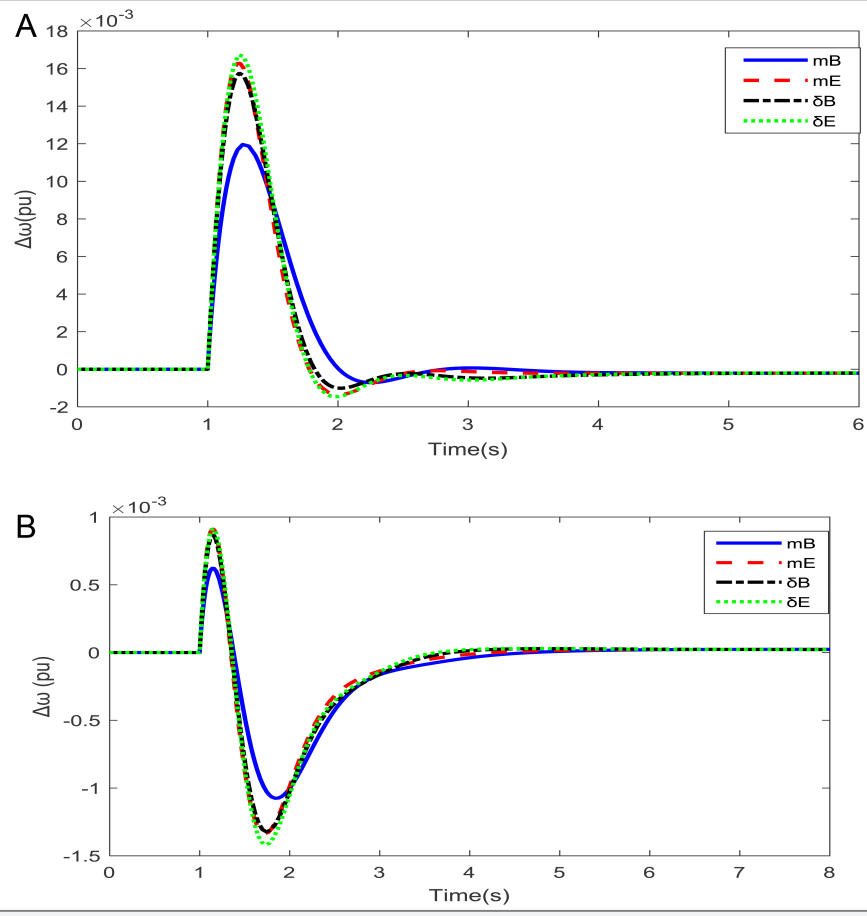

Fig. 15. (a) Speed deviation response for step increase in Pm and (b) Speed deviation response for step decrease in Pm under Case V.

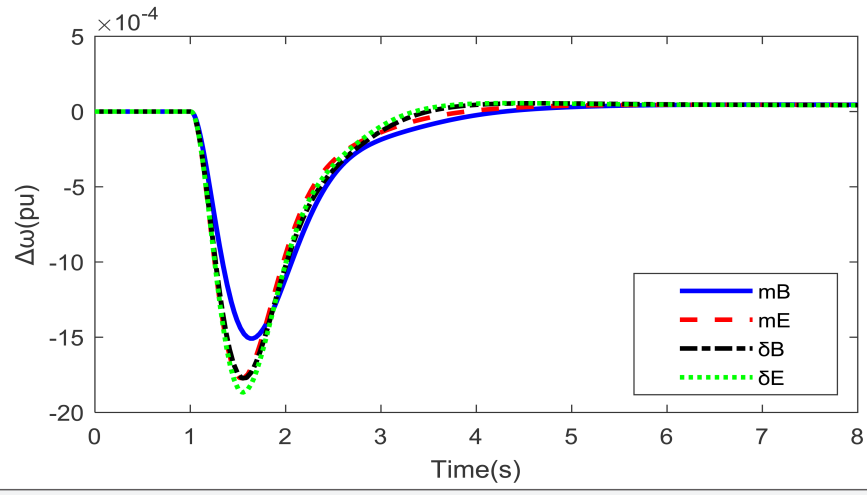

Fig. 16. Speed deviation response for Case VI (step rise in Vref).

5) Case IX: Variation of System Parameters in T2FLL-Based UPFC Controller: In order to assess the robustness and effectiveness of the T2FLL-based UPFC damping controller, the machine's inertia constant and the system's open circuit direct axis transient time constant are both decreased by 25% and 30%, respectively. The system responses of speed deviation under the above disturbances of mB, mE, δB δE signal of each cases of T2FL -based UPFC controller power system as shown in Fig. 17a and b. It is observed from the Fig. 17a and b that the system responses of speed deviation all the four alternatives maintain stability but however for the case of m_B signal T2FLL based UPFC damping controller gives better transient performances as compared to mE, δB δE signal of same controller and same poer system four alternatives.

VI. CONCLUSION

- This paper has been a systematic approach for designing the linear model and developed the simulation test model of UPFC-based

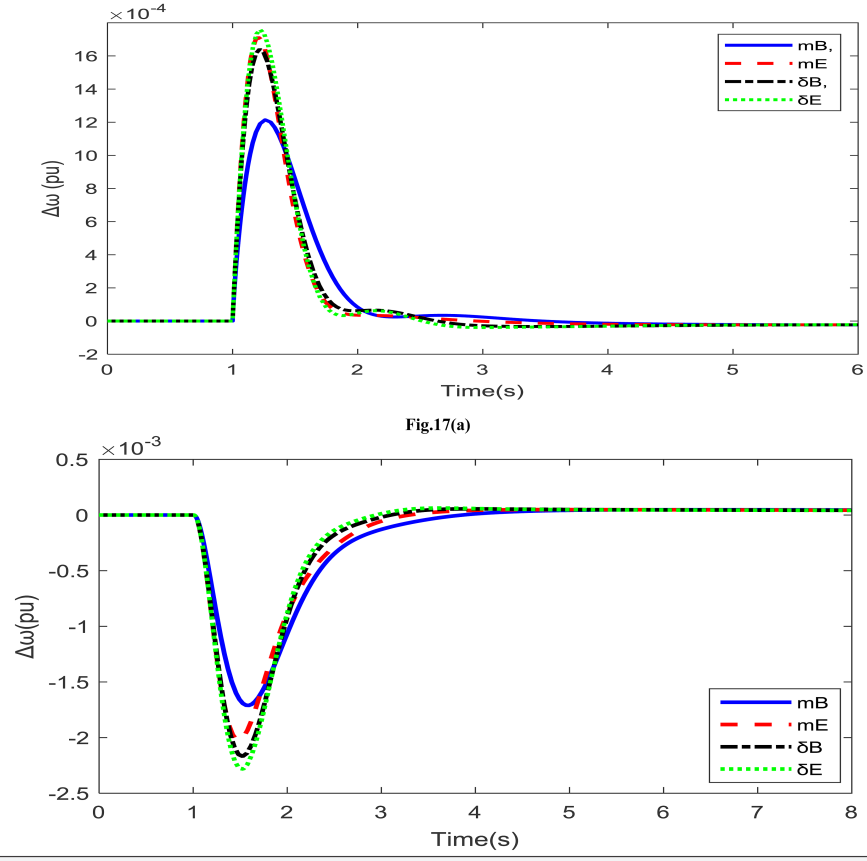

Fig. 17. (a) Speed deviation response for (25% drop in M) and (b) Speed deviation response for (30% reduction in T'do) under Case VII.

damping controller in SMIB power system. The proposed power system model is initially demonstrated in PD type LL-based UPFC damping controller which is employed separately for WMFOA, WOA, MFO, and PSO optimization algorithm for computational efforts of the system. The analysis shows that the m_B-based PD type LL UPFC damping controller has the least ITAE value as compared to δ_B, m_E, and δ_E-based PD type LL UPFC of the same power system. It is observed from the demostration that WMFOA optimized in PD type LL based UPFC damping controller the percentage reduction of ITAE value as compared to WOA, MFO, and PSO optimized same controller of the same power system. The percentage reduction of ITAE value in WMFOA as compared to MFO, WOA, and PSO optimized of the same controller is 32.28%, 42.41%, and 48.72%, respectively.

- It is observed from the demonstration under step disturbance of mechanical power input in the system that WMFOA optimized design of PD type LL-based UPFC damping controller gives superior damping performances of low-frequency oscillation as compared to WOA, MFO, and PSO optimized design tuning controller parameters of same power system.
- The eigenvalue analysis is demonstrating the effectiveness of the PD type LL controller of the proposed power system. It is investigated that time domain simulation results effectively dampen the low-frequency oscillations in WMFOA-based optimization design of PD type LL controller as compared to MFO, WOA, and PSO-based PD type LL controller of the same power system. It is clear that tuning of the proposed WMFOA-based UPFC PD type LL controller is a very good ability to dampen low-frequency oscillations in the power systems and significantly improve their transient stability.
- The WMFOA-optimized design of the T2FLL-based UPFC damping controller power system is compared with the PD type LL-based UPFC controller of the same power system in the second phase of the analysis of the proposed work. It is clear that the least value of ITAE value is obtained in m_B-based T2FLL UPFC controller as compared to m_E, δ_B, δ_E-based T2FLL UPFC-based controller of the same power system. It is noted that MFOA optimized m_B signal T2FLL based UPFC damping controller the percentage of ITAE value decrease 38.19%, 45.03%, and 47.44% respectively as compared to m_E, δ_B, δ_E each signal of T2FLL based UPFC controller of the same power system , . It is clear that m_B-based T2FLL UPFC damping controller employed MFOA optimized outperforms as compared to m_E, δ_B, δ_E-based T2FLL UPFC damping controller of the same power system.
- It is also observed that T2FLL based UPFC damping controller gives the better transient stability performances as compared to PD typ eLL based UPFC damping controller of the same system under different fault condition of the power system.
- The study also demonstrated the transient stability performances of the proposed system under four alternatives such that modulation index and phase angle m_B, m_E, δ_B, and δ_E of T2FLL-based UPFC controller in the power system under different fault conditions and change of parameters in the system. It is observed that T2FLL with m_B-UPFC-based damping controller gives better performances as compared to among the four input control signals to the T2FLL-based same UPFC controller of the power system.
- The future scope of the proposed work is the multi-machine power system and a new type of controller can be attempted for better improvement of transient stability of the performances of the system.

Peer-review: Externally peer-reviewed.

Author Contributions: Concept – S.K.M., S.K.B.; Design – S.K.M., S.K.B.; Supervision – S.K.M., S.K.B.; Resources – S.K.M., S.K.B.; Materials – S.K.M., S.K.B.; Data Collection and/or Processing – S.K.M., S.K.B.; Analysis and/or Interpretation – S.K.M.; Literature Search – S.K.B.; Writing – S.K.M., S.K.B.; Critical Review – S.K.M.

Declaration of Interests: The author declare that they have no competing interest.

Funding: The authors declared that this study has received no financial support.

REFERENCES

1. P. Kundur, *Power System Stability and Control*. New York: McGraw-Hill, 1994.
2. N. G. Hingorani, and L. Gyugyi, *Understanding FACTS: Concepts and Technology of Flexible AC Transmission Systems*. New York: IEEE Press, 2000.
3. Y. H. Song, and T. A. Johns, *Flexible AC Transmission Systems*. London: IEE, 2000.
4. L. Gyugyi, "Unified power flow control concept for Flexible ac Transmission Systems," *IEE Proc. C Gener. Transm. Distrib. UK*, vol. 139, no. 4, pp. 323–331, 1992. [CrossRef]
5. L. Gyugyi, C. D. Schauder, S. L. Williams, T. R. Rietman, D. R. Torgerson, and A. Edris, "The unified power flow controller: A new approach to power transmission control," *IEEE Trans. Power Delivery*, vol.10, no. 2, pp.1085–1097, 1995. [CrossRef]
6. E. Raajeshwar, and A. Jeevanaandham, *Improving Transient Stability of Power System Using UPFC with PID and POD Controllers*. IEEE Publications, 2017. [CrossRef]
7. S. Ghaedi, S. Abazari, and G. A. Markadeh, "Transient stability improvement of power system with UPFC control by using transient energy function and sliding mode observer based on locally measurable information," *Measurement*, vol.183, p. 109842, 2021. [CrossRef]
8. H. Fujita, Y. Watanabe, and H. Akagi, "Transient analysis of a unified power flow controller and its application to design of the DC-link capacitor," *IEEE Trans. Power Electron.*, vol.16, no.5, pp.735–740, 2001. [CrossRef]
9. P. S. Georgilakis, and N. D. Hatziargyriou, "Unified power flow controllers in smart power systems: Models, methods, and future research," *IET Smart Grid*, vol. 2, No. 1, pp.2–10, 2019. [CrossRef]
10. D. Kobibi, Y. I. Hadjeri Samir, D. Mohamed, "Modelling a UPFC for the study of power system steady state and transient characteristics," *Int. J. Adv. Eng. Sci.*, vol. 3, no.1, pp.124–133, 2014.
11. M. Ebeed, S. Kamel, J. Yu, and F. Jurado, "Development of UPFC operating constraints enforcement approach for power flow control," *IET Gener. Transm. Distrib.*, vol.13, no.-20, pp.4579–4591, 2019. [CrossRef]
12. A. M. Shotorbani, A. Ajami, M. P. Aghababa, and S. H. Hosseini"Direct Lyapunov theory-based method for power oscillation damping by robust finite-time control of unified power flow controller" *IET Gener. Transm. Distrib.*, vol. 7, no. 7, pp. 691–699, 2013. [CrossRef]
13. S. Shojaeian, J. Soltani, and G. A. Markadeh, "Damping of low frequency oscillations of multi-machine multi-UPFC power systems, based on adaptive input-output feedback linearization control," *IEEE Trans. Power Syst.*, vol. 27, no. 4, pp. 1831–1840, 2012. [CrossRef]
14. B. K. Dubey, and N. K. Singh, "Multimachine power system stability enhancement with UPFC using linear QUADRATIC regulator techniques," *Int. J. Adv. Res. Eng. Technol.*, vol.11, No.-4, pp.219–229, 2020.
15. N.Nahak, S. Bohidar, and R. K. Mallick, "Investigation of UPFC based damping controller parameter for power oscillation damping by grey-wolf optimizer with time delay for multi machine system," *IREACO*, vol.11, no.1, 2018. [CrossRef]
16. B. V. Kumar, G. Rajendar, and V. Ramaiah, "Optimal location and capacity of unified power flow controller based on chaotic krill herd blended runner root algorithm for dynamic stability improvement in power system," *Int. J. Numer. Modell. Electron. Netw.*, vol. 34, no. 2, 2021.
17. J. Liu, Z. Xu, J. Yang, and Z. Zhang, "Modeling and analysis for global and local power flow operation rules of UPFC embedded system under typical operation conditions," *IEEE Access*, vol.8, pp.21728–21741, 2020. [CrossRef]
18. H. F. Wang, "Damping function of unified power flow controller," *IEE Proc. Gener. Transm. Distrib.*, vol.146, no.1, pp.81–87, 1999. [CrossRef]

19. P. K. Dash, S. Mishra, and G. Panda, "A radial basis function neural network controller for UPFC," *IEEE Trans. Power Syst.*, vol. 15, no. 4, pp. 1293–1299, 2000. [CrossRef]
20. B. C. Pal, "Robust damping of inter area oscillations with unified power flow controller," *IEE Proc. Gener. Transm. Distrib.*, vol. 149, no. 6, pp. 733–738, 2002. [CrossRef]
21. S.Tiwari, R. Naresh, and R. Jha, "Neural network predictive control of UPFC for improving transient stability performance of power system," *Appl. Soft Comput.*, vol. 11, no. 8, pp. 4581–4590, 2011. [CrossRef]
22. S. Limyingcharone, U. D. Annakkage, and N. C. Pahalawaththa, "Fuzzy logic based unified power flow controllers for transient stability improvement," *IEE Proc. Gener. Transm. Distrib.*, vol. 145, no. 3, pp. 225–232, 1998. [CrossRef]
23. N. Nahaka, and R. K. Mallick, "Enhancement of small signal stability of power system using UPFC based damping controller with novel optimized fuzzy PID controller," *J. Intell. Fuzzy Syst.*, vol. 35, no. 1, pp. 501–512, 2018. [CrossRef]
24. V. P. Rajderkar, and V. K. Chandrakar, "Design Coordination of a fuzzy-based Unified Power Flow Controller with hybrid energy storage for enriching power system dynamics," *Eng. Technol. Appl. Sci. Res.*, vol. 13, no. 1, pp. 10027–10032, 2023. [CrossRef]
25. S. Latha, and C. K. Rani, "Transient stability improvement with unified power flow controller using fuzzy logic and ANFIS Approach," *Adv. Mater. Res.*, vol. 768, pp. 378–387, 2013. [CrossRef]
26. P. K. Dash, S. Mishra, and G. Panda, "A radial basis function neural network controller for UPFC," *IEEE Trans. Power Syst.*, vol. 15, no. 4, pp. 1293–1299, 2000. [CrossRef]
27. V. K. Chandrakar, and A. G. Kothari, "Fuzzy logic based unified power flow controllers for improving transient stability," *Int. J. Power Energy Syst.*, vol. 28, no. 2, pp. 135–144, 2008. [CrossRef]
28. P. Farhadi, M. Ziaei, M.Bayati, E.Ramezani, and T.Sojoudi, "Fuzzy control performance on unified power flow controller to increase power system stability," 4th International Conference on Power Engineering, Energy and Electrical Drives Istanbul, Turkey, May 13–17, 2013. [CrossRef]
29. J. G. Singh et al., *Development of a Fuzzy Rule Based Generalized Unified Power Flow Controller, European Transactions on Electrical Power*, vol. 19, no. 5, 2008, pp.702–717.
30. W. Fang, and H. W. Ngan, "Enhancing small signal power system stability by coordinating unified power flow controller with power system stabilizer," *Electr. Power Syst. Res.*, vol. 65, no. 2, pp. 91–99, 2003. [CrossRef]
31. H. Shayeghi, H. A. Shayanfar, S. Jalilzadeh, and A. Safari, "Design of output feedback UPFC controller for damping of electromechanical oscillations using PSO," *Energy Convers. Manag.*, vol. 50, no. 10, pp. 2554–2561, 2009. [CrossRef]
32. H. Shayeghi, H. A. Shayanfar, S. Jalilzadeh, and A. Safari, "Tuning of damping controller for UPFC using quantum particle swarm optimizer," *Energy Convers. Manag.*, vol. 51, no. 11, pp. 2299–2306, 2010. [CrossRef]
33. H. Shayeghi , H. A. Shayanfar , S. Jalilzadeh , and A. Safari, "COA based robust output feedback UPFC controller design," *Energy Convers. Manag.*, vol. 51, no. 12, pp. 2678–2684, 2010. [CrossRef]
34. R. K. Khadanga, and J. K. Satapathy, "A new hybrid GA-GSA algorithm for tuning damping controller parameters for a unified power flow controller," *Electr. Power Energy Syst.*, vol. 73, pp. 1060–1069, 2015.
35. S. R. Paital, P. K. Ray, and S. R. Mohanty, "A robust dual interval type-2 fuzzy lead–lag based UPFC for stability enhancement using Harris Hawks Optimization," *ISA Trans.*, vol. 123, pp. 425–442, 2022. [CrossRef]
36. N. Nahaka, and R. K. Mallick, "Damping of power system oscillations by a novel DE-GWO optimized dual UPFC controller," *Eng. Sci. Technol. An Int. J.*, vol. 20, no. 4, pp. 1275–1284, 2017. [CrossRef]
37. S. A. Al-Mawsawi, A. Haider, and S. A. Al-Qallaf, "Multivariable controller design for unified power flow controller using evolutionary optimization algorithms," *WSEAS Trans. Syst. Control*, vol.12, pp.277–287, 2017.
38. M. Eslami, H. Shareef, M. R. Taha, and M. Khajezadeh, "Adaptive particle swarm optimization for simultaneous design of UPFC damping controllers," *Electr. Power Energy Syst.*, vol. 57, pp. 116–128, 2014. [CrossRef]
39. M. H. Nadimi-Shahraki et al., "Hybridizing of whale and moth-flame optimization algorithms to solve diverse scales of optimal power flow problem," *Electron. MDPI*, vol. 11, no. 831, 2022.
40. S. Mirjalili, "Moth-flame optimization algorithm: A novel nature-inspired heuristic paradigm," *Knowl. Based Syst.*, vol. 89, pp. 228–249, 2015. [CrossRef]
41. R. H. Bhesdadiya, I. N. Trivedi, P. Jangir, and N. Jangir, "Moth-flame optimizer method for solving constrained engineering optimization problems," In *Advances in Computer and Computational Sciences*, vol. 554. Singapore: Springer, 2018, pp. 61–68. [CrossRef]
42. S.Saurav,V. K.Gupta,and S. K.Mishra, "Moth-flame optimization-based algorithm for FACTS devices allocation in a power system," International Conference on Innovations in Information, Embedded and Communication Systems, 2017. [CrossRef]
43. M.Nadeem *et al.* "Optimal placement, sizing and coordination of FACTS devices in transmission network using whale optimization algorithm," *Energies*, vol. 13, no. 3, p. 753, 2020. [CrossRef]
44. I. S.Shahbudin et.al., "FACTS device installation in transmission system using whale optimization algorithm," *Bulletin EEI*, vol. 8, no. 1, pp. 30–38. [CrossRef]
45. S. Panda, N. K. Yegireddy, and S. K. Mohapatra, "Hybrid BFOA–PSO approach for coordinated design of PSS and SSSC-based controller considering time delays," *Int. J. Electr. Power Energy Syst.*, vol. 49, pp. 221–233, 2013. [CrossRef]
46. S. K. Mohapatra, and S. Panda, "Stability enhancement with SSSC-based controller design in presence of non-linear voltage-dependent load," *Int. J. Intell. Syst. Technol. Appl.*, vol. 15, no. 2, pp. 163–187, 2016. [CrossRef]
47. M. A. Taher, S. Kamel, and Y. Juan, "Optimal locations and sizes of shunt FACT devices for enhancing power system load ability using improved moth flame optimization," *Electr. Power Compon. Syst.*, vol. 49, no. 20, pp. 1536–1554, 2022.
48. S. Mirjalili, and A. Lewis, "The whale optimization algorithm," *Adv. Eng. Softw.*, vol. 95, pp. 51–67, 2016. [CrossRef]
49. P. R. Sahu, P. K. Hota, S. Panda, R. K. Lenka, S. K. Padmanaban, and F. Blaabjerg, "Coordinated design of FACTS controller with PSS for stability enhancement using a novel hybrid whale optimization algorithm-nelder mead approach," *Electr. Power Compon. Syst.*, vol. 49, no. 16–17, 2021.

Mr. Sanat Kumar Barik Graduated in Electrical Engineering in 2002, M.E Degree in Electrical Engineering in 2006 and presently he is working as Assistant Professor in Electrical Engineering, Seemanta Engineering College, Mayurbhanj, Odisha and Research scholar under BPUT, Odisha. His research interests are the field of Electrical power system and control, Optimization techniques, Flexible AC Transmission System.

Dr. Sangram Keshori Mohapatra received BE degree in Electrical Engineering in the year 1999, M.Tech degree in the year of 2008 in the specialization of Power Electronics and Drives and Ph.D degree in the year of 2014 in the specialization of power system Engineering. He has acquired more than 22 years of experience in the field of Academics and Research pertaining to Electrical Engineering. Presently, he is working as an Associate Professor in Electrical Engineering, Government College of Engineering, Keonjhar a constituent college of BPUT, Odisha. He has published about 60 papers in international journal and conferences. He has guided 25 M.Tech research scholars .He is currently guiding 4 Ph.D Research scholars. He is the Life member of Indian Society for Technical Education (ISTE), India and Fellow of The Intuitions of Engineers (IEI) and member of IEEE and reviewer of various repute journal. His research interest is in the area of flexible AC transmission systems (FACTS), modeling of machines, power electronics, power systems and FACTS, controller design, power system stability, optimization Techniques. and Automatic generation and control.

APPENDIX. SYSTEM DATA ARE IN PU UNLESS SPECIFIED OTHERWISE

Generator	M = 8 MJ/MVA	$X_d = 1$	$X_q = 0.6$	$X'_d = 0.3$
	$T'_{do} = 5.044$	$V_t = V_b = 1$	$D = 0$	$P_e = 0.8$
Excitor	$K_A = 100$	$TA = 0.01s$		
Transformer	$X_{tE} = 0.1$	$X_E = X_B = 0.1$		
Transmission line	$X_{Bv} = 0.3$	$X_e = 0.5$		
UPFC Controller	$m_E = 0.4013$	$m_B = 0.0789$	$\delta_E = -85.3478^0$	$\delta_B = -78.2174^0$
	VDC = 2	$C_{DC} = 1$		